Article

Intestinal Gpr17 deficiency improves glucose metabolism by promoting GLP-1 secretion

Shijun Yan,[1,2] Jason M. Conley,[1,2] Austin M. Reilly,[1,3] Natalie D. Stull,[9] Surabhi D. Abhyankar,[1,5] Aaron C. Ericsson,[11] Tatsuyoshi Kono,[2] Andrei I. Molosh,[3,8] Chandrashekhar A. Kubal,[7] Carmella Evans-Molina,[1,2,10] and Hongxia Ren[1,2,3,4,5,6,12,*]

[1]Herman B. Wells Center for Pediatric Research, Department of Pediatrics, Indiana University School of Medicine, Indianapolis, IN 46202, USA
[2]Center for Diabetes and Metabolic Diseases, Indiana University School of Medicine, Indianapolis, IN 46202, USA
[3]Medical Neuroscience Graduate Program, Stark Neurosciences Research Institute, Indiana University School of Medicine, Indianapolis, IN 46202, USA
[4]Department of Anatomy, Cell Biology and Physiology, Indiana University School of Medicine, Indianapolis, IN 46202, USA
[5]Department of Biochemistry and Molecular Biology, Indiana University School of Medicine, Indianapolis, IN 46202, USA
[6]Department of Pharmacology & Toxicology, Indiana University School of Medicine, Indianapolis, IN 46202, USA
[7]Department of Surgery, Indiana University School of Medicine, Indianapolis, IN 46202, USA
[8]Department of Psychiatry, Institute of Psychiatric Research, Indiana University School of Medicine, Indianapolis, IN 46202, USA
[9]Indiana Biosciences Research Institute, Indianapolis, IN 46202, USA
[10]Richard L. Roudebush VA Medical Center, Indianapolis, IN 46202, USA
[11]Metagenomics Center, University of Missouri, Columbia, MO 65201, USA
[12]Lead contact
*Correspondence: renh@iu.edu
https://doi.org/10.1016/j.celrep.2021.110179

SUMMARY

G protein-coupled receptors (GPCRs) in intestinal enteroendocrine cells (EECs) respond to nutritional, neural, and microbial cues and modulate the release of gut hormones. Here we show that Gpr17, an orphan GPCR, is co-expressed in glucagon-like peptide-1 (GLP-1)-expressing EECs in human and rodent intestinal epithelium. Acute genetic ablation of Gpr17 in intestinal epithelium improves glucose tolerance and glucose-stimulated insulin secretion (GSIS). Importantly, inducible knockout (iKO) mice and Gpr17 null intestinal organoids respond to glucose or lipid ingestion with increased secretion of GLP-1, but not the other incretin glucose-dependent insulinotropic polypeptide (GIP). In an *in vitro* EEC model, overexpression or agonism of Gpr17 reduces voltage-gated calcium currents and decreases cyclic AMP (cAMP) production, and these are two critical factors regulating GLP-1 secretion. Together, our work shows that intestinal Gpr17 signaling functions as an inhibitory pathway for GLP-1 secretion in EECs, suggesting intestinal GPR17 is a potential target for diabetes and obesity intervention.

INTRODUCTION

Enteroendocrine cells (EECs) in the gastrointestinal (GI) tract sense luminal content and release gut hormones, which regulate glucose metabolism and feeding through endocrine and neuronal mechanisms (Gribble and Reimann, 2016; Kim et al., 2018; Schwartz and Zeltser, 2013). The postprandial glucose lowering effect of incretin hormones is often blunted in type 2 diabetes (T2D) and enhanced after bariatric surgery (Douros et al., 2019; Nauck et al., 1986). Glucagon-like peptide-1 (GLP-1) is an incretin hormone secreted by preproglucagon-expressing EECs (traditionally named L cells) and is degraded rapidly by dipeptidylpeptidase 4 (DPP4) (Holst, 2007). Long-acting GLP-1 analogs and DPP4 inhibitors have been developed for the treatment of T2D (Drucker and Nauck, 2006). A potential alternative treatment strategy for T2D is through the modulation of endogenous GLP-1 secretion; however, the factors and path-ways involved in the regulation of endogenous GLP-1 secretion remain incompletely understood.

G protein-coupled receptors (GPCRs) regulate GLP-1 secretion in EECs by responding to the rise of nutrients (e.g., lipids, carbohydrates, and peptides), molecules associated with food ingestion (e.g., bile acids), and hormonal and neural factors (e.g., somatostatin, calcium, and endocannabinoids) (Reimann et al., 2012), which in turn activate downstream signaling pathways that regulate gut hormone secretion through second messengers (Ezcurra et al., 2013). As GPCRs are the target of more than a quarter of the Food and Drug Administration-approved drugs (Hauser et al., 2017), understanding the biological actions of GPCRs in EECs will likely provide insight into developing new diabetes therapeutics by promoting endogenous GLP-1 secretion.

GPR17 was initially identified as an orphan GPCR phylogenetically related to purinergic and cysteinyl-leukotriene (CysLT) receptors (Ciana et al., 2006; Parravicini et al., 2008) with an
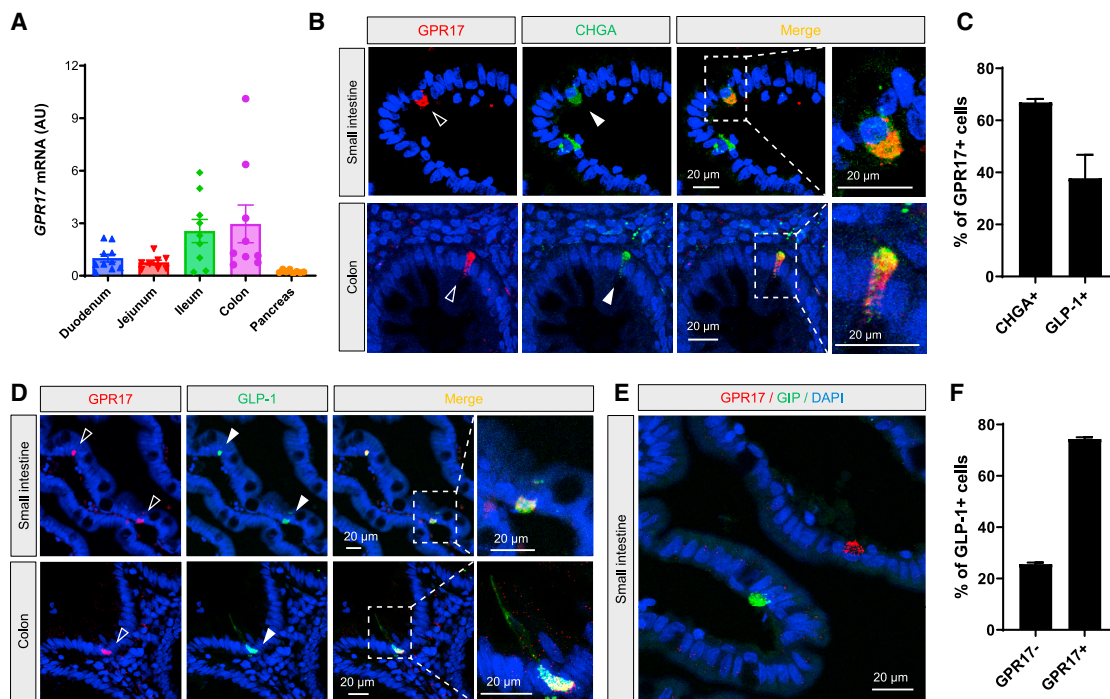
Figure 1. Co-expression of GPR17 and GLP-1 in EECs in human intestine

(A) qRT-PCR result of *GPR17* mRNA in human gut segments and pancreas (n = 8–10). Gene expression was calculated as $2^{-\Delta\Delta ct}$. *RPLP0* was used as an internal control.

(B) Co-immunostaining of GPR17 and CHGA, a pan-EEC marker, in human small intestine (top) and colon (bottom).

(C) Co-immunostaining of GPR17 and GLP-1 in human small intestine (top) and colon (bottom).

(D) Co-immunostaining of GPR17 and GIP in human small intestine.

(E) Quantification of cells expressing CHGA in GPR17 + cells (n = 117 cells from two human samples were analyzed), and cells expressing GLP-1 in GPR17 + cells (n = 282 cells were analyzed).

(F) Quantification of cells expressing GPR17 in GLP-1-producing cells (n = 181 cells from two human samples were analyzed).

Data are displayed as means ± SEM. See also Figure S1.

implicated function in oligodendrocyte myelination (Ceruti et al., 2009; Chen et al., 2009; Lecca et al., 2008). We previously identified Gpr17 as the transcriptional target of Forkhead box protein O1 (FoxO1) in hypothalamic neurons and demonstrated its physiological role in maintaining metabolic homeostasis (Reilly et al., 2019; Ren et al., 2015; Ren et al., 2012). In this study, we first made the exciting discovery of GPR17 expression in GLP-1-producing EECs in the GI tract. We further evaluated the metabolic function of intestinal Gpr17 by generating constitutive and inducible intestinal Gpr17 knockout mouse models and characterized Gpr17 downstream signaling pathways in cultured EECs and intestinal organoids. Our results suggest that intestinal GPR17 contributes to the regulation of glucose metabolism by modulating GLP-1 secretion.

RESULTS

GPR17 is expressed in GLP-1-producing cells in human and mouse gut epithelium

Existing data within the Genotype-Tissue Expression (GTEx) portal demonstrated the expression of *GPR17* mRNA in human intestinal tissues (https://www.gtexportal.org/home/gene/GPR17#geneExpression). Our qRT-PCR showed human *GPR17*

expression increased from the proximal to the distal intestine (Figure 1A), similar to the expression pattern of preproglucagon gene *GCG* (Mojsov et al., 1986). Interestingly, we detected GPR17 expression in flask-shaped cells resembling EECs in the intestinal epithelium by immunohistochemistry (IHC), but not in the submucosa or muscular layers (Figure S1A). To characterize the GPR17-positive cells, we first performed double staining using chromogranin A (CHGA) as a pan-EEC marker (Figure 1B). Our quantified result showed that the majority (66.9%) of GPR17-positive cells were also CHGA positive in human intestine (Figure 1E). Next, we examined if GPR17 was enriched in a subtype of EECs. We found that GPR17 was co-expressed with GLP-1 (Figure 1C), and the majority of GLP-1-producing cells (74.4%) were GPR17 positive (Figure 1F). However, GPR17 was not observed in glucose-dependent insulinotropic polypeptide (GIP)-producing cells in human small intestine (Figure 1D). As antibody specificity is often a concern for GPCR antibodies (Michel et al., 2009), we validated the commercial GPR17 antibody by performing double staining in permeabilized HEK293 cells transiently expressing an HA epitope-tagged human GPR17 construct. Anti-HA and anti-GPR17 antibody staining overlapped in the same cells (Figure S1B). GPR17 antibody staining overlapped with more than 90% of HA antibody staining cells (Figures S1C and S1D)
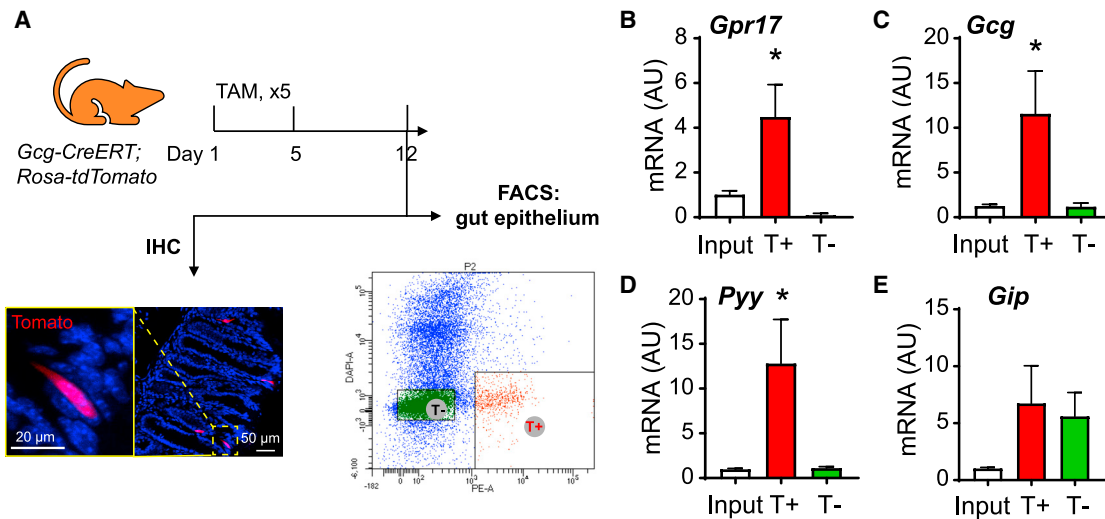
Figure 2. Enrichment of Gpr17 in GLP-1-producing cells in mouse intestine
(A) FACS of intestine epithelial cells dissociated from *Gcg-CreERT;Rosa-tdTomato* mouse post tamoxifen injection. *Gcg*-expressing cells were labeled by red fluorescence (tdTomato) and sorted by FACS within 1 week after tamoxifen treatment (2 mg/d for 5 days by oral gavage).
(B–E) qRT-PCR analysis of *Gpr17* (B), *Gcg* (C), *Pyy* (D), and *Gip* (E) mRNA in sorted cells (n = 7 mice). Gene expression was calculated as 2^-ΔΔct. β-actin was used as an internal control. Gene expression was expressed relative to input fractions. Unpaired two-tailed Student's t test, *p < 0.05. Data are displayed as means ± SEM.

with minimal nonspecific staining (Figure S1E), thereby validating the GPR17 antibody used in our study. Since a substantial fraction of GPR17 staining was detected intracellularly in the permeabilized cells (Figures S1B–S1F), we examined the nonpermeabilized cells and found colocalization of anti-HA and anti-GPR17 staining on the cell surface (Figure S1G).

We further substantiated our findings using sorted mouse intestinal GLP-1-producing EECs. We crossed *Gcg-CreERT* mice (Shiota et al., 2017) with *Rosa-tdTomato* reporter mice to label GLP-1-producing cells. With tamoxifen-induced Cre expression, GLP-1-producing cells were labeled by tdTomato (Figure 2A) and collected by fluorescence-activated cell sorting (FACS) (T+ fraction in Figure 2A). The qRT-PCR result showed that *Gpr17* transcripts were enriched in T+ cells (Figure 2B). Consistent with previous reports of transcriptional profiles of GLP-1-producing cells (Habib et al., 2012), we also observed enriched transcripts of *Gcg* (encoding preproprotein that is eventually cleaved into glucagon-like peptides including GLP-1 and GLP-2 in intestine) and *Pyy* (encoding peptide YY), but not *Gip* (Figures 2C–2E). Together, these results indicated that GPR17 was expressed in most GLP-1-producing cells in the gut epithelium.

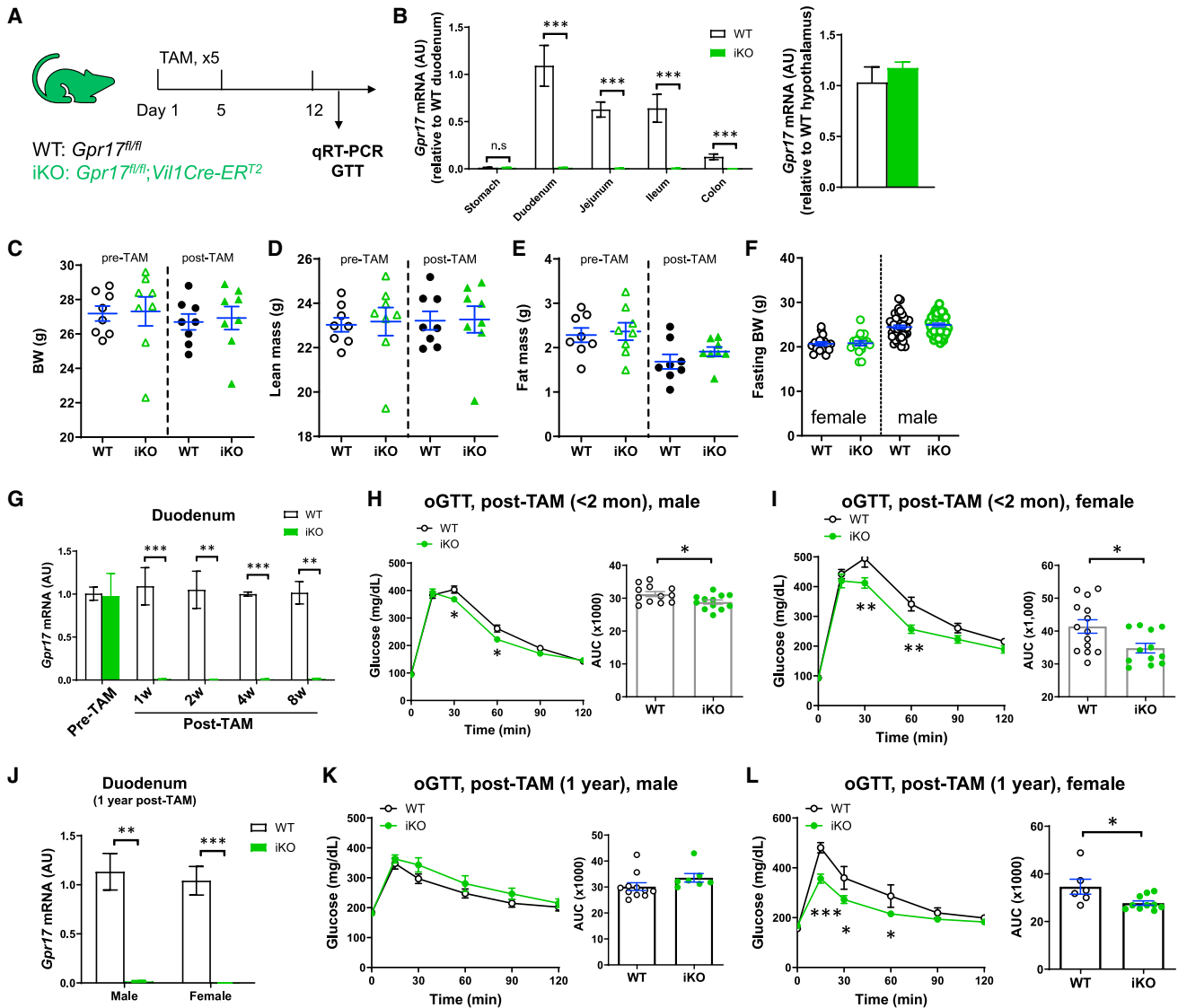## Inducible intestine-specific Gpr17 knockout mice had improved glucose tolerance

To elucidate the metabolic function of intestinal Gpr17, we generated tamoxifen (TAM)-inducible intestine-specific *Gpr17* knockout mice (*Gpr17^fl/fl^; Vil1Cre-ER^T2^*; namely iKO hereafter) (Figure 3A). The *Gcg-Cre* guided GLP-1-producing cell-specific *Gpr17* knockout mice are not suitable for our study. There are two major reasons: (1) *Gcg-cre* is activated not only in gut but also in any tissues expressing *Gcg*, such as islets (Figures S2C and S2D) and the nucleus tractus solitarius of the brain stem (Kat-

surada and Yada, 2016) (data not shown); (2) due to the constant gut epithelial renewal, the Gpr17-deficient GLP-1-producing cells were quickly replaced by the newly regenerated GLP-1-producing cells with intact *Gpr17* alleles, once the tamoxifen injection was terminated (Figures S2A and S2B). However, *Vil-Cre* under the control of the *villin* promotor targeted epithelial progenitor cells throughout the digestive epithelium and persisted throughout adulthood, despite rapid intestinal cell renewal (el Marjou et al., 2004). Therefore, we bred *Gpr17^fl/fl^* mice with *Vil1Cre-ER^T2^* mice to generate inducible gut epithelium-specific *Gpr17* knockout mice for our studies.

After tamoxifen injection, *Gpr17* expression was almost completely abolished in the small intestine and colon of iKO mice, but not in the stomach or hypothalamus (Figure 3B). The body weight and composition of iKO mice were comparable to those of the wild-type (WT) control before and after tamoxifen treatments (Figures 3C–3E). There was no difference in fasting body weight before glucose tolerance testing in WT and iKO mice (Figure 3F). The genetic knockout was sustained after the initial tamoxifen injection (Figure 3G). Within 8 weeks after tamoxifen-induced *Gpr17* genetic ablation, male iKO mice showed significantly improved oral glucose tolerance (Figure 3H). Similarly, female iKO mice showed even greater significant improvement in glucose tolerance after *Gpr17* genetic ablation (Figure 3I). Furthermore, after long-term Gpr17 genetic ablation (1 year post tamoxifen injection) (Figure 3J), female (Figure 3L) but not male mice (Figure 3K) still displayed significantly improved glucose tolerance.

Knocking out intestinal Gpr17 increased nutrient-stimulated insulin and GLP-1 secretion *in vivo*

To address how intestinal Gpr17 deficiency led to improved glucose metabolism in iKO mice, we examined insulin secretion

Figure 3. Inducible intestine-specific Gpr17 knockout mice displayed improved glucose tolerance

(A) Experimental setup for inducible intestinal Gpr17 knockout mice. $Gpr17^{fl/fl}$ (WT) and $Gpr17^{fl/fl};Vil1Cre-ER^{T2}$ (iKO) mice were subjected to experiments at least 1 week after tamoxifen treatment (2 mg/d for 5 days by oral gavage).

(B) Gpr17 mRNA expression in mouse gut and hypothalamus from iKO (n = 9) and WT (n = 6) mice at 1 week after tamoxifen injection. Gene expression was calculated as 2˜-ΔΔct. β-actin was used as an internal control. p values were calculated by unpaired two-tailed Student's t test.

(C–E). Body weight (C), lean mass percent (D), and fat mass percent (E) of male mice before and after tamoxifen injection (n = 8 mice for each group).

(F) Fasting body weight before glucose tolerance tests (n = 17~50 mice for each group).

(G) Time course study measuring Gpr17 mRNA in duodenum following tamoxifen injection (n = 3 mice). p values were calculated with unpaired two-tailed Student's t test.

(H) Oral glucose tolerance (oGTT, 3 g/kg) in overnight-fasted male iKO (n = 12) and WT (n = 12) mice within 2 months after tamoxifen injection.

(I) oGTT (3 g/kg) in overnight-fasted female iKO (n = 14) and WT (n = 12) mice within 2 months after tamoxifen injection.

(J) Gpr17 mRNA in duodenum in WT and iKO mice 1 year after initial tamoxifen injection.

(K) oGTT (3 g/kg) in 4-h-fasted male iKO (n = 7) and WT (n = 11) mice 1 year after tamoxifen injection.

(L) oGTT (3 g/kg) in 4-h-fasted female iKO (n = 10) and WT (n = 6) mice 1 year after tamoxifen injection.

Two-way ANOVA and unpaired two-tailed Student's t test were performed for glucose curve and AUC, respectively. *p < 0.05, **p < 0.01, ***p < 0.001. Data are displayed as means ± SEM. See also Figure S2.

using the oral glucose-stimulated insulin secretion (GSIS) assay. Both female and male iKO mice responded to oral glucose gavage with increased serum insulin levels (Figures 4A and 4F). Incretin

hormones play important roles in regulating insulin secretion in pancreatic islet β-cells (Campbell and Drucker, 2013), and we have observed Gpr17 expression in GLP-1-producing EECs
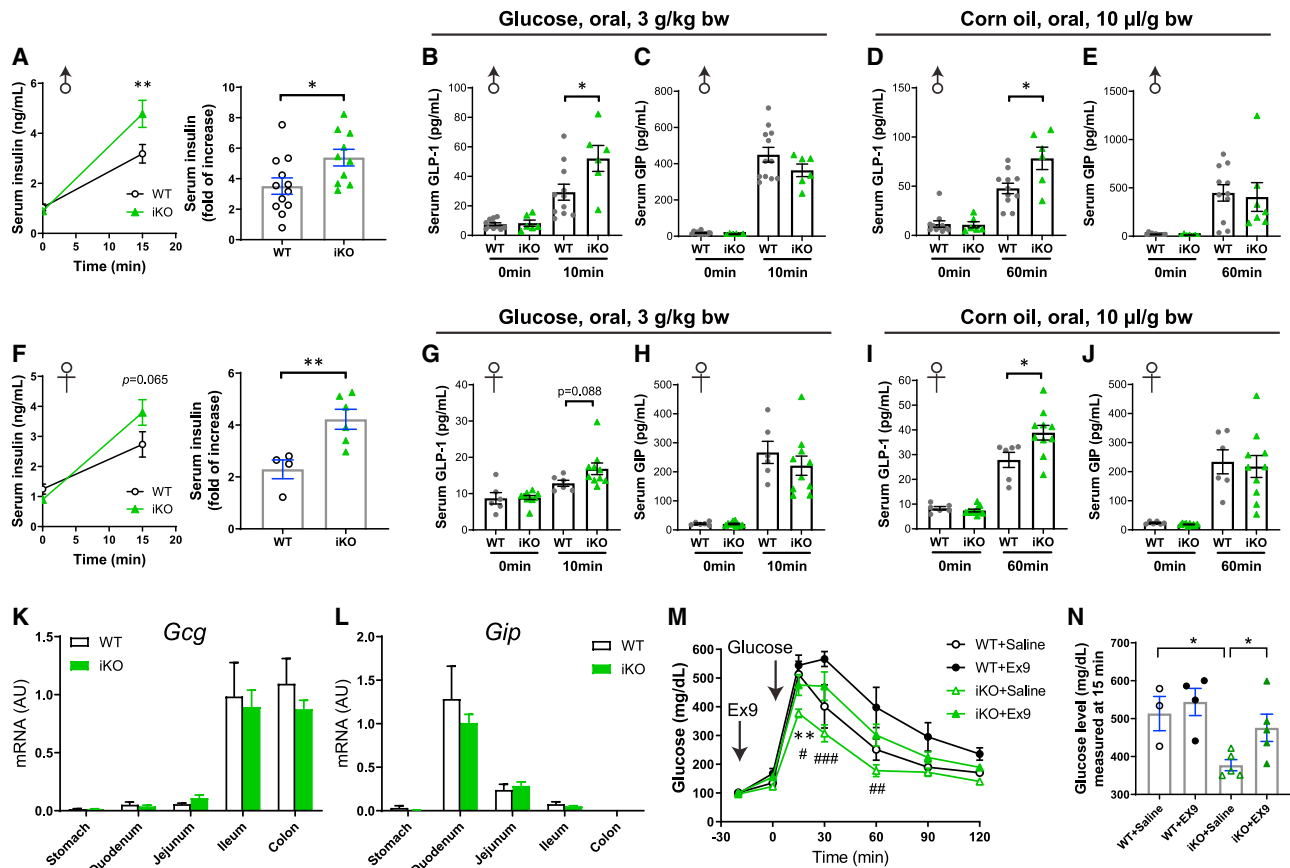
Figure 4. Gpr17 deficiency enhanced insulin and GLP-1 secretion in response to nutrients *in vivo*

(A) Oral glucose-stimulated insulin secretion (oGSIS) in overnight-fasted male iKO mice versus WT mice after tamoxifen injection (post-TAM). Serum insulin levels were measured before and 15 min after an oral glucose load (3 g/kg) (n = 10–12 mice). Unpaired two-tailed Student's t test was performed.

(B and C) Plasma total GLP-1 (B) and GIP (C) levels in response to an oral glucose load (3 g/kg) in male inducible intestinal Gpr17 deficient mice (iKO, n = 6) and WT mice (n = 11). Tail blood samples were collected at 0 min and 10 min after oral glucose intake in 4∼6 h fasted mice. Two-way ANOVA was performed.

(D and E) Plasma total GLP-1 (D) and GIP (E) levels in response to an oral corn oil load (10 μL/g) in male inducible intestinal Gpr17 deficient mice (iKO, n = 6) and WT mice (n = 11). Tail blood samples were collected at 0 min and 60 min after oral glucose intake in 4∼6 h fasted mice. Two-way ANOVA was performed.

(F) Oral glucose-stimulated insulin secretion (oGSIS) in overnight-fasted female iKO mice versus WT mice after tamoxifen injection (post-TAM). Serum insulin levels were measured before and 15 min after an oral glucose load (3 g/kg) (n = 4∼6 mice). Unpaired two-tailed Student's t test was performed.

(G and H) Plasma total GLP-1 (G) and GIP (H) levels in response to an oral glucose load (3 g/kg) in female iKO mice (n = 10) and WT mice (n = 6). Tail blood samples were collected at 0 min and 10 min after oral glucose intake in 4∼6 h fasted mice. Two-way ANOVA was performed.

(I and J) Plasma total GLP-1 (I) and GIP (J) levels in response to an oral corn oil load (10 μL/g) in female iKO mice (iKO, n = 10) and WT mice (n = 6). Tail blood samples were collected at 0 min and 60 min after oral glucose intake in 4∼6 h fasted mice. Two-way ANOVA was performed.

(K and L) *Gcg* (K) and *Gip* (L) mRNA levels in the gut of inducible Gpr17 deficient mice (iKO) by qRT-PCR (n = 6∼9 mice).

(M) ipGTT (3 g/kg) in mice pretreated with GLP-1R antagonist exendin-(9–39) (Ex9, 10μg, [I]p.) (n = 3∼5 mice). Two-way ANOVA, *p < 0.05 WT + Saline versus iKO + Saline. #p < 0.05, ##p < 0.01 iKO + Saline vs iKO + Ex9.

(N) Blood glucose levels at 15 min time point in ipGTT. Unpaired two-tailed Student's t test was performed.

*p < 0.05, **p < 0.01, ***p < 0.001. Data are displayed as means ± SEM.

(Figures 1 and 2). We hypothesized that knocking out intestinal Gpr17 increases GLP-1 secretion in response to nutrient ingestion. To test this, we measured incretin (GLP-1 and GIP) secretion in iKO and WT mice during fasting and after nutrient administration. Fasting GLP-1 (0 min, Figures 4B and 4D) and GIP (0 min, Figures 4C and 4E) levels had no difference between male WT and iKO mice. Ten minutes after oral glucose dosing, plasma total GLP-1 levels in iKO male mice were greater than those in WT mice (Figure 4B), while GIP levels were comparable between the two groups (Figure 4C). Meanwhile, iKO males responded to

oral corn oil dosing with higher concentrations of total GLP-1 (Figure 4D) and similar GIP levels (Figure 4E). Female iKO mice showed a trend of more GLP-1 secretion after glucose gavage, although this finding was not statistically significant (p = 0.088, Figure 4G). Furthermore, female iKO mice responded to oral corn oil dosing with higher GLP-1 secretion (Figure 4I). Female iKO mice had comparable GIP secretion to WT mice after either oral glucose or corn oil gavage (Figures 4H and 4J). Neither fasting GLP-1 (0 min, Figures 4G and 4I) nor fasting GIP (0 min, Figures 4H and 4J) levels were different in female iKO mice compared with

WT mice. In addition, we did not detect any significant changes in *Gcg* or *Gip* transcripts in intestinal Gpr17 knockout mice (Figures 4K and 4L).

To further substantiate our finding, we tested whether injection of Ex9, a GLP-1 receptor antagonist, could dampen the improvement of glucose metabolism in iKO mice. We administrated Ex9 at a dose of 10 μg/mouse, which is 20% of the dose that has been previously shown to induce significant glucose intolerance in WT mice (Burmeister et al., 2017; Chambers et al., 2017). As expected, compared with the mild effect on intraperitoneal glucose tolerance test (ipGTT) in WT mice, Ex9 at 10 μg/mouse exerted more profound impact on iKO mice (Figure 4M). Notably, 15 min after glucose dosing, iKO + Ex9 group had significantly higher blood glucose than iKO + saline group (Figure 4N). These data demonstrate that knocking out intestinal Gpr17 improved glucose tolerance through, at least in part, the mechanisms of promoting GLP-1 secretion in response to nutrient ingestion *in vivo*.

Intestinal Gpr17 deficiency did not affect gut morphology, islets, or gut microbiota

We next determined whether changes in gut morphology, pancreatic islet, and/or gut microbiota may contribute to the glucose phenotype observed in Gpr17 knockout mice. The general morphology of small intestine and colon in adult iKO mice (4 months after TAM injection) was no different compared with WT mice (Figures 5A–5D). The villi and crypt length in iKO small intestine were similar to those of WT (Figures 5B and 5C). The thickness of colonic epithelium (including surface epithelium and crypts) was also comparable between iKO and WT mice (Figure 5E). The size and number of pancreatic islets were not altered in iKO mice compared with WT mice examined by IHC with insulin staining (Figures 5F–5H).

The gut microbiome is one of the integral factors for maintaining metabolic homeostasis *in vivo* (Quigley, 2013). We examined if knocking out intestinal Gpr17 led to changes in gut microbiota composition and found no significant difference in the composition and diversity of gut microbiome (Figures S3A–S3F). Heatmaps arranged using hierarchical clustering methods and principal component analysis of bacteria showed no gene factor-induced difference in WT and iKO fecal samples (Figures S3G and S3H). Therefore, we conclude that acutely knocking out intestinal Gpr17 caused no change in bacterial composition, richness, or diversity of the gut microbiota.

### Enhanced GLP-1 secretion in Gpr17 null intestinal organoids

We further investigated the effect of Gpr17 deficiency on incretin secretion using intestinal organoid, a three-dimensional *ex vivo* mini-gut that retains the architectural complexity and cellular diversity of gut epithelium (Sato et al., 2009). To obtain *Gpr17* null organoids, we first generated constitutive intestinal Gpr17 knockout mice (*Gpr17^{fl/fl};Vil1Cre*) and then derived the Gpr17 null intestinal organoids from these mice. We detected a significant reduction (approximately 90%) of *Gpr17* mRNA in duodenum and negligible levels of *Gpr17* mRNA expression in other intestinal segments (jejunum, ileum, and colon) of the knockout mice (Figure 6A). qRT-PCR confirmed the lack of *Gpr17* in organoids derived from intestinal Gpr17 knockouts (Figures 6B and 6C), while neither

Gcg nor *Gip* transcription was affected (Figure 6D). Interestingly, *Gpr17* null organoids had significantly increased GLP-1 secretion under basal condition with 1 mmol/L glucose, while GIP secretion remained unchanged (Figure 6E). When stimulated with palmitoleic acid (Figure 6F), a monounsaturated fatty acid, and GPBAR-A (Figure 6G), an agonist of bile acid receptor (G-protein-coupled bile acid receptor [GPBAR]), *Gpr17* null organoids demonstrated increased GLP-1, but not GIP secretion. When stimulated with forskolin (adenylyl cyclase activator) and 3-Isobutyl-1-methylxanthine (IBMX, phosphodiesterase inhibitor) (Fsk/IBMX), GLP-1 (Figure 6H), but not GIP (Figure 6I), secretion was elevated in *Gpr17* null organoids with forskolin at indicated concentrations.

Gpr17 deficiency enhanced GLP-1 secretion in cultured GLUTag cells through the Ca^{2+} and cAMP signaling pathways

Our data showed that intestinal Gpr17 knockout led to better glucose metabolism via increased GLP-1 and insulin secretion *in vivo*. However, the exact molecular mechanisms are still unclear. To answer this question, we used *in vitro* cultured GLUTag cells, an established murine intestinal EEC line that secretes GLP-1 in a regulated manner (Brubaker et al., 1998; Drucker et al., 1994). The rise of intracellular calcium triggers exocytosis in various cell types, including neurons (Pang and Südhof, 2010), pancreatic beta cells (Satin, 2000), and EECs (Kuhre et al., 2015). We used whole-cell patch clamp to monitor the currents of voltage-dependent calcium channels (VDCCs) (Figures 7A and 7B). Overexpressing Gpr17 (GFP + cells) in GLUTag cells resulted in reduced amplitude of Ca^{2+} current triggered by membrane depolarization with *I/V* curve shown in Figure 7C and area under the curve (AUC) shown in Figure 7D. No difference regarding cell capacitance between transfected cell and non-transfected cells was observed (Figure 7E). Reduced amplitude of Ca^{2+} current indicated less Ca^{2+} flux into intracellular space when Gpr17-expressing EECs responded to nutrient stimulation.

The cAMP signaling pathway is well known to potentiate Ca^{2+}-induced exocytosis in a variety of secretory cells including EECs (Ezcurra et al., 2013; Seino and Shibasaki, 2005). We measured cAMP levels in live GLUTag cells cotransfected with GloSensor, a cAMP biosensor (Buccioni et al., 2011), and mouse Gpr17 (mGpr17) to determine whether Gpr17 regulates cAMP generation in EECs. The cAMP level was lower in cells expressing mGpr17 as compared with empty vector, suggesting constitutive activity consistent with Gαi coupling (Figure 7F). Treatment with the synthetic GPR17 agonist, MDL29,951, had concentration-dependent effects on the cAMP response in cells expressing mGpr17 (Figure 7F). Specifically, a biphasic pattern was observed where inhibition of cAMP was detected for MDL29,951 concentrations between ~10 nM and 300 nM, but stimulation of cAMP was observed at MDL29,951 concentrations ≥ ~30 μM. GloSensor cAMP signal differences were also observed between empty vector and mGpr17-expressing cells upon addition of 3 μM forskolin (Figure 7G), suggesting constitutive receptor activity suppressing cAMP levels in these cells. MDL29,951 further inhibited the forskolin-stimulated GloSensor cAMP response in a concentration-dependent manner (Figure 7G). However, MDL29,951 had no effect on GloSensor cAMP responses in empty vector-transfected cells (Figure 7G), suggesting that the effects of MDL29,951 are
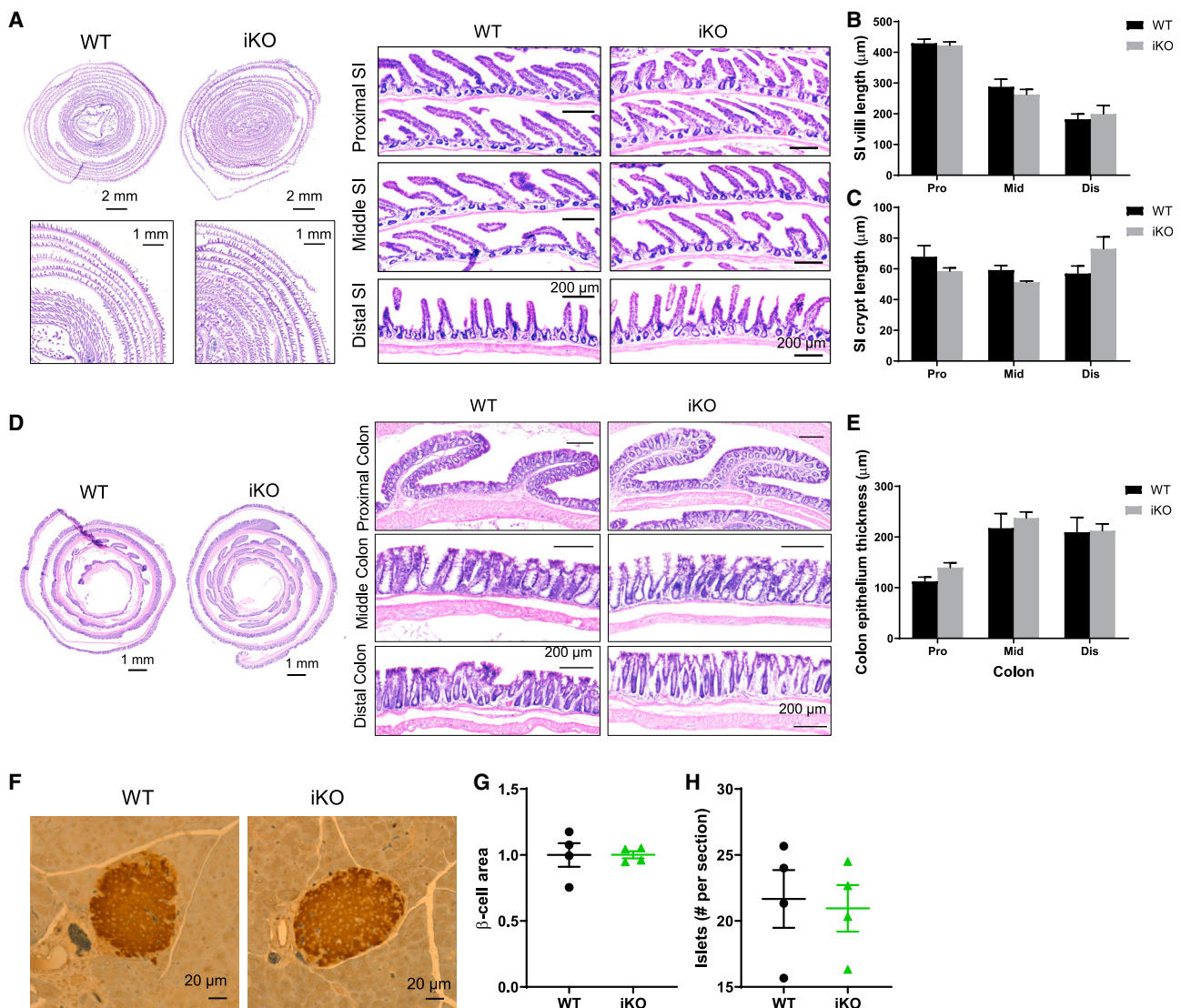
Figure 5. Gpr17 deficiency did not affect gut morphology and islets in intestinal Gpr17 KO mice

(A–C) H&E staining showing the histology of small intestine (A). Villi (B) and crypt length (C) were quantified; 8~25 villi and crypts for each segment were measured per mouse. Data show the average of three mice for each group.

(D and E) H&E staining showing the histology of colon (D). Colon epithelium thickness (E) (including surface epithelium and crypts) was quantified (n = 3 mice); 9~17 spots for each segment were measured per mouse. Data show the average of three mice for each group.

(F–H) IHC staining of mouse pancreas (WT and iKO) using insulin antibody (n = 4 mice) (F). β-cell size (G) and amount (H) were quantified. Unpaired two-tailed Student's t tests were performed.

Data are displayed as means ± SEM. See also Figure S3.

mediated by mGpr17. Time course recording showed that MDL29,951 inhibited forskolin-stimulated induction of luminescence in GLUTag cells expressing mGpr17 (Figures 7H and 7I). Taken together, these experiments suggest that mGpr17 expression constitutively inhibits cAMP levels in GLUTag cells through Gαi-coupling. Furthermore, agonist activation of mGpr17 had biphasic effects on basal cAMP levels that were dependent on MDL29,951 concentration, but exclusively inhibitory effects on forskolin-stimulated cAMP.

Activation of several GPCRs could directly inhibit VDCCs (Ruiz-Velasco and Ikeda, 2000; Sun et al., 2001) and cAMP production

(Robichaux and Cheng, 2018) via Gβγ and Gαi subunits, respectively. To directly prove the Gαi/Gβγ coupling of GPR17, we performed bioluminescence resonance energy transfer (BRET) assay in HEK293 cells transiently expressing TRUPATH Gαβγ biosensor (Olsen et al., 2020). BRET was reduced in mGpr17-expressing cells, but not in empty vector- or human neurotensin receptor type 1 (NT1R)-expressing cells, when treated with 100 nM MDL29,951 (Figure 7J), suggesting GPR17 was coupled to Gαi and its activation could induce Gαi/Gβγ dissociation.

In summary, we showed that GPR17 acts as a brake to negatively regulate GLP-1 secretion in EECs by inhibiting Ca²⁺
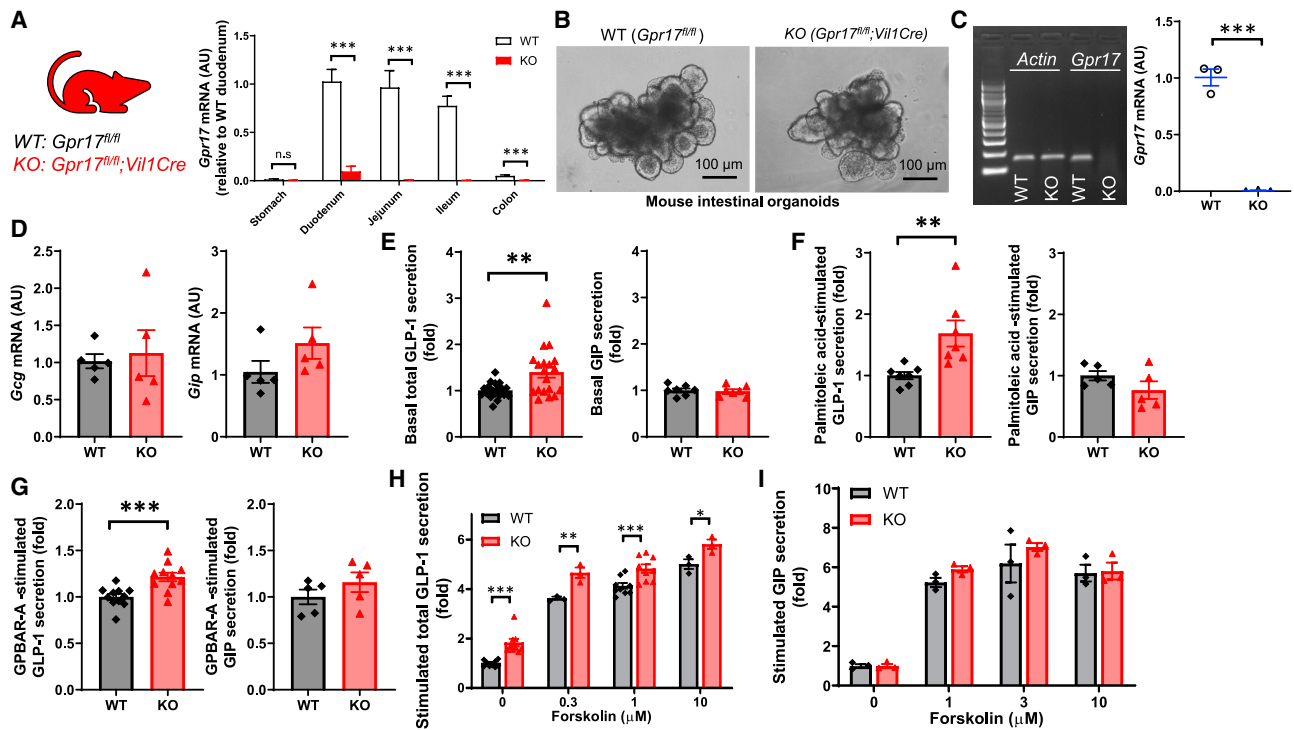
Figure 6. GLP-1 secretion is enhanced in Gpr17-deficient intestinal organoids derived from *Gpr17^{fl/fl};Vil1Cre* mice

(A) *Gpr17* mRNA expression in the gut of *Gpr17^{fl/fl}* (WT) and *Gpr17^{fl/fl};Vil1Cre* (KO) mice. Gene expression was calculated as 2^-ΔΔct. β-actin was used as an internal control. Gene expression was expressed relative to duodenum (n = 5 mice for WT, n = 10 mice for KO). Unpaired t tests were performed for statistical analysis.

(B) Bright-field images of intestinal organoids derived from adult WT and constitutive Gpr17 KO mice.

(C) qRT-PCR of *Gpr17* mRNA in organoids (n = 3 mice). Gene expression was normalized to β-actin. Representative gel electrophoresis image of qRT-PCR products was shown. Unpaired two-tailed Student's t test was performed.

(D) qRT-PCR of *Gcg* and *Gip* mRNA in organoids (n = 5 mice).

(E) GLP-1 (n = 19 replicates for each group) and GIP (n = 7 replicates for each group) secretion from intestinal organoids under basal conditions (1 mmol/L glucose) for 2 h. Unpaired two-tailed Student's t test was performed.

(F) Gpr17 deficiency enhanced fatty acid-induced GLP-1 secretion (n = 7 replicates for each group), but not GIP (n = 5 replicates for each group). Organoids were incubated with palmitoleic acid, a monounsaturated fatty acid, at 40 μmol/L for 2 h.

(G) Gpr17 deficiency enhanced bile acid receptor agonist-induced GLP-1 secretion (n = 11 replicates for each group), but not GIP (n = 5 replicates for each group). Organoids were incubated with GPBAR-A, an agonist of bile acid receptor (TGR5), at 20 μmol/L for 2 h.

(H and I) Gpr17 deficiency enhanced cAMP-elevating agents-induced GLP-1 secretion (n = 3∼13 replicates) (H), but not GIP (n = 3 replicates) (I). Organoids were incubated with cAMP-elevating agents, forskolin (0, 0.3, 1, 3, and 10 μmol/L) and 10 μmol/L IBMX for 2 h. p values were calculated using two-way ANOVA test. Percentage of GLP-1 secretion was calculated by measuring GLP-1 levels in the supernatants and cell lysates and normalized to WT organoids in parallel on the same day. Data were obtained from at least three independent experiments.

*p < 0.05, **p < 0.01, ***p < 0.001. Data are displayed as means ± SEM.

signaling and cAMP generation in response to nutrient stimulation (Figure 7K). Inhibition of GPR17 signaling could potentiate nutrient-stimulated GLP-1 secretion, and consequently improve glycemic control *in vivo*.

DISCUSSION

GLP-1 and GIP are incretin hormones secreted by enteroendocrine cells in the intestinal epithelial lining within minutes after meal ingestion (Ezcurra et al., 2013; Holst, 2007). GLP-1 and GIP regulate glucose homeostasis and appetite via endocrine and neural mechanisms (Kim et al., 2018; Steinert et al., 2017). In T2D, the overall incretin effect is reduced (Nauck et al., 1986). The cellular mechanisms and intestinal luminal cues governing endogenous

GLP-1 secretion are subjects of intense investigation yet remain poorly understood. Here we demonstrated that an orphan GPCR, GPR17, was expressed in GLP-1-producing enteroendocrine cells in the human and rodent intestinal epithelium using complementary approaches (IHC- and FACS-based gene expression characterization). The presence of GPR17 in intestine and its colocalization with GLP-1 led us to further evaluate its previously unrecognized physiological roles in glucose metabolism. We generated the acute inducible (iKO) intestine-specific Gpr17 loss-of-function mouse models. Both female and male iKO mice showed improved glucose tolerance with increased oral GSIS. Furthermore, iKO mice also responded to oral nutrient (glucose or lipid) ingestion with increased GLP-1 secretion. Finally, our *in vitro* studies showed that Gpr17 signaling in cultured EECs
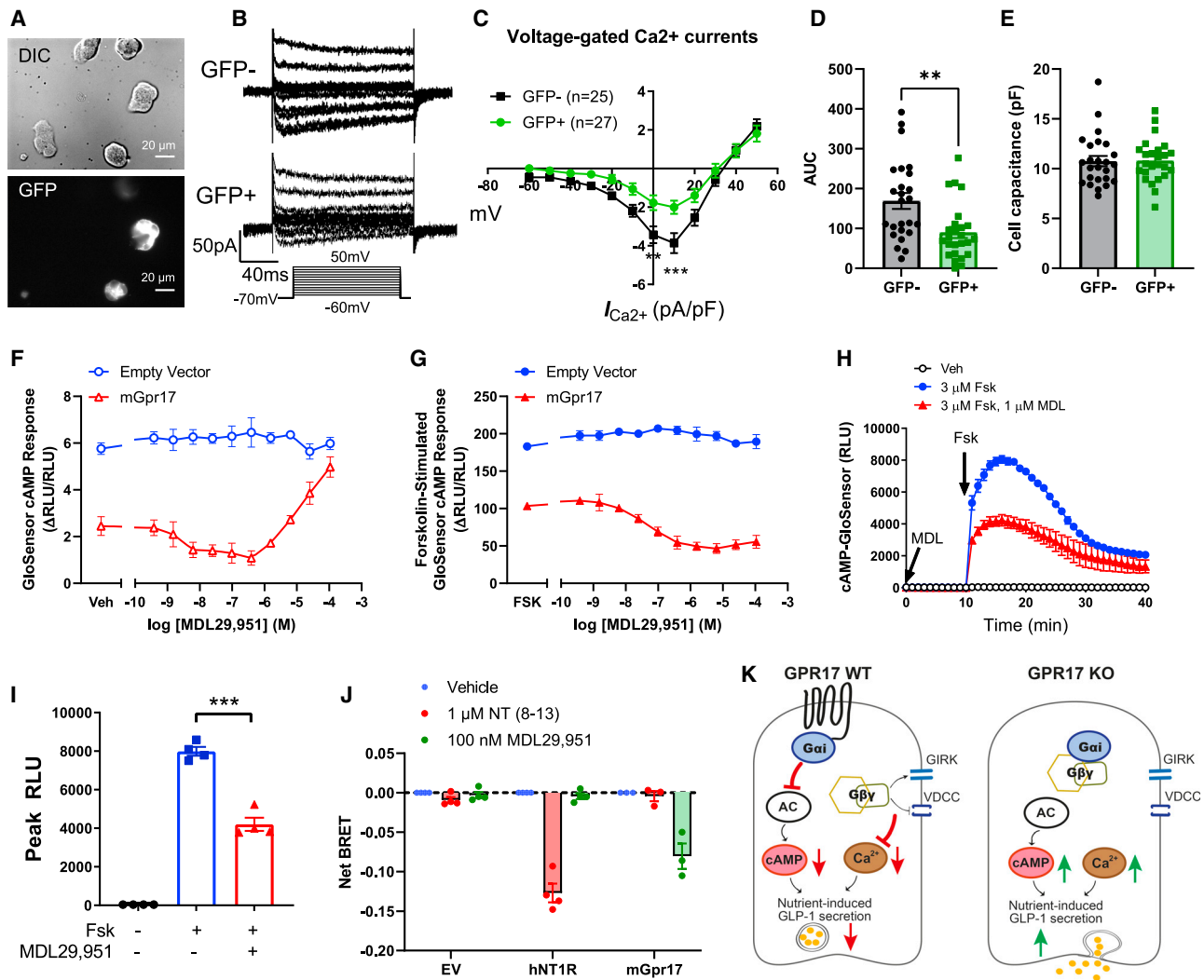
Figure 7. Gpr17 regulates GLP-1 secretion through Ca^{2+} and cAMP signaling

(A) Whole-cell patch clamp recording voltage-gated Ca^{2+} currents in GLUTag cells that were transiently transfected with pcDNA3.1-mGpr17-GFP. All cells were patched under IR-DIC optics and GFP-positive cells were identified by using an upright microscope fitted with fluorescence optics.

(B) Ca^{2+} current responses to 150 ms voltage steps of 10 mV increments from a holding potential of −70 mV. The inset shows the voltage pulse protocol. Tetrodotoxin (TTX) at 0.3 μmol/L was added to block Na$^+$ currents.

(C) Current–voltage relationship of the voltage-gated Ca^{2+} currents recorded in Gpr17-overexpressed GLUTag cells (GFP+; n = 27 cells) and nontransfected cells (GFP−; n = 25 cells). Statistical comparisons between groups in were performed using two-way ANOVA and Sidak's post hoc tests.

(D) Averaged AUC for voltage-current curve of Ca^{2+} currents.

(E) Cell capacitance were comparable between Gpr17-overexpressed GLUTag cells (GFP+) and nontransfected cells (GFP−).

(F) Gpr17 expression and agonist stimulation, MDL29,951, inhibited GloSensor cAMP response in GLUTag cells without forskolin addition.

(G) Gpr17 expression and MDL29,951 inhibited forskolin-stimulated GloSensor cAMP response in a concentration-dependent manner in GLUTag cells. Data for (F) and (G) were represented as the mean ± SEM of two independent experiments performed with duplicate wells.

(H and I) Time course recording showing MDL29,951 inhibited forskolin-stimulated cAMP response in mouse Gpr17-overexpressing GLUTag cells (n = 4 replicates) (H). Peak RLU were quantified (I). Vehicle (Veh) or MDL29,951 (1 μmol/L) were incubated for 10 min before forskolin addition. Unpaired two-tailed Student's t test was performed.

(J) GPR17-Gαi/Gβγ coupling is identified by TRUPATH in HEK293 cells transiently transfected with either pcDNA3.1 (−) empty vector, pcDNA3.1 (+)-hNT1R, or pcDNA3-HA-mGpr17 together with pcDNA5/FRT/TO-Gαi1-Rluc8, pcDNA3.1-Gβ3, and pcDNA3.1-Gγ9-GFP2. The net BRET response represents the BRET ratio for each well subtracted by the mean BRET ratio response of the vehicle-treated wells for each receptor transfection condition. hNT1R, human neurotensin receptor type 1. Data are represented as the mean ± SEM of three or four independent experiments performed with triplicate wells.

(K) Schematic diagram illustrates the molecular mechanisms of how GPR17 negatively regulates nutrient-induced GLP-1 secretion in EECs. GPR17 signals through Gαi pathway to reduce cAMP production in enteroendocrine cells, in turn dampening nutrient-stimulated cAMP rise and Ca^{2+}-stimulated exocytosis. Gβγ subunits released from Gαi reduce Ca^{2+} influx upon nutrient stimulation through activation of G-Protein-Coupled Inwardly Rectifying Potassium (GIRK) channels and inhibition of VDCCs. On the other hand, GPR17 deficiency increases cAMP and intracellular Ca^{2+} rise, thereby potentiating nutrient-induced GLP-1 secretion.

*p < 0.05, **p < 0.01, ***p < 0.001. Data are displayed as means ± SEM.

inhibited Ca^{2+} influx and cAMP production via coupling with Gαi. Gpr17 null intestinal organoids also showed increased GLP-1 secretion. Collectively, these findings demonstrated that inhibiting intestinal Gpr17 signaling improved glucose metabolism via potentiating nutrient-induced GLP-1 secretion from enteroendocrine cells.

GPCRs constitute a large family of proteins that engage in regulating various physiological responses by sensing a diverse array of ligands and coupling with discrete downstream cellular signaling cascades. For instance, GPCRs expressed in EECs can be activated by luminal nutrients, microbiome metabolites, and basolateral stimulations from the enteric nervous system or the circulation (Hauser et al., 2017; Husted et al., 2017; Mace et al., 2015). Efforts have been made to identify EEC-specific GPCRs (Haber et al., 2017; Panaro et al., 2014), though sequencing depth and library preparation often impose limitations to detect GPCR transcripts with low abundance in single-cell RNA sequencing (scRNAseq) studies (Mawla and Huising, 2019; Wang and Kaestner, 2019). We took direct experimental approaches and found Gpr17 mRNA and protein expression in the GLP-1-producing EECs of the rodent and human gut epithelium. Our *in vivo* physiological and *in vitro* molecular mechanism studies supported our hypothesis that Gpr17 intestinal knockout improves glucose homeostasis by promoting GLP-1 secretion. In addition to demonstrating increased GLP-1 secretion in iKO mice and organoids, we unbiasedly tested and subsequently ruled out the following alternative hypotheses. First, the improved glucose tolerance phenotype is not secondary to defects in nutrient intake, as Gpr17 intestinal iKO mice exhibited normal weight, body composition, and gut morphology with *ad libitum* feeding on normal chow diet. Second, we performed extensive profiling and found no difference in the gut microbiota composition of Gpr17 intestinal iKO mice. Last, the number and size of the pancreatic islets in the acute Gpr17 intestinal iKO mice were comparable to the measurements of the WT mice. Taken together, the results from these control experiments further strengthen our initial hypothesis that intestinal Gpr17 plays an important role in glucose homeostasis by modulating GLP-1 secretion.

We previously identified Gpr17 as an effector of FoxO1 orexigenic signals in the brain (Ren et al., 2012). Loss of Gpr17 in the brain confers increased hypothalamic neuronal sensitivity to insulin and leptin, leading to reduced *ad libitum* feeding and increased relative energy expenditure (Ren et al., 2015). Other groups reported that loss of Gpr17 mitigates brain damage through a FoxO-dependent mechanism (Lecca et al., 2008; Marschallinger et al., 2015). In the intestine, we reason that FoxO1 is less likely to mediate the effects GPR17, since FoxO1 expression was restricted in the chromogranin A-positive endocrine cells and serotonin (5HT)-positive cells, but not GLP-1-producing cells (Bouchi et al., 2014). Moreover, knocking out Gpr17 is less likely to affect the transcription factor upstream. Indeed, in our inducible Gpr17 knockout mice, Gpr17 ablation did not cause a compensatory increase of FoxO1 transcripts in the intestine (data not shown).

As a result of physiological compensation and developmental adaption, germ-line knockout models of established metabolic factors often showed lack of body weight phenotype or surprisingly milder glucose phenotype (Qian et al., 2002; Scrocchi et al., 1996; Scrocchi and Drucker, 1998), which limits the inter-

pretation of negative data as a true absence of function (Chambers et al., 2013). This could be the case for the lack of phenotype in one Gpr17 germ-line knockout model (Mastaitis et al., 2015), although another study reported beneficial metabolic effects (Ou et al., 2019). Being aware of the potential confounding factors of germ-line knockout approaches, we tested the inducible tissue-specific knockouts in our studies. Our inducible intestine-specific knockout mice yielded largely consistent phenotypes for both sexes and revealed metabolic functions of Gpr17 signaling in the gut that are distinct from our previously reported role in the brain. Therefore, we speculate that inhibiting Gpr17 signaling in brain and gut yields concerted improvement of metabolic outcomes through different cellular mechanisms and complementary endocrine pathways.

In gut EECs, our data revealed that GLP-1 secretion was regulated by GPR17 and the downstream signaling pathways mediated via G protein subunits: Gαi and G$\beta\gamma$ (Figure 7K). Previous Gpr17 signaling studies using the heterologous expression models have yielded complicated and sometimes even paradoxical results (Ciana et al., 2006; Hennen et al., 2013; Simon et al., 2016). Adding to the complexity of the issue, GPCRs in metabolic organs have the capacity to signal through multiple pathways in cell-type-specific manners, and it is often not clear which pathway is associated with a given biological effect for a particular receptor (Husted et al., 2017). To better understand the physiological function of GPR17, we used physiologically relevant models, including inducible tissue-specific knockout animals, intestinal organoids, and cultured EECs. Our results indicate that GPR17 engaged Gαi signaling pathway is physiologically relevant for regulating incretin secretion in the enteroendocrine cells. First, Gαi subunits released from the coupled GPCR directly inhibit adenylyl cyclase activity and consequently reduce cAMP production. Second, G$\beta\gamma$ subunits released from Gαi modulate membrane potential through activation of G protein-gated inwardly rectifying K$^+$ channels (GIRKs) and inhibition of voltage-dependent Ca^{2+} channels (VDCCs) (Lüscher and Slesinger, 2010; Smrcka, 2008; Sun et al., 2001). In the voltage-clamp setting, which would bypass the modulation of Ca^{2+}-influx through GIRK-channel, we found GPR17 overexpression inhibited voltage-gated Ca^{2+} channels, suggesting the constitutive activation of GPR17 could directly inhibit VDCCs. The activation of Gαi-coupled GPCR causes voltage-dependent inhibition of Ca^{2+} channels (Bean, 1989; Ikeda and Dunlap, 1999) mediated by G$\beta\gamma$ subunits (Ruiz-Velasco and Ikeda, 2000), a process that has been well documented in neuronal cells (Dunlap et al., 1995). Given the many shared features of neuronal transmitter release in neurons and gut hormone secretion in EECs, we hypothesized that activation of GPR17 could directly modulate voltage-gated Ca^{2+} channels through G$\beta\gamma$ subunits in EECs. Gpr17 signaling through the Gαi/G$\beta\gamma$ pathway has been reported in several articles (Ciana et al., 2006; Hennen et al., 2013; Inoue et al., 2019; Merten et al., 2018; Simon et al., 2016). Furthermore, by application of G$\alpha\beta\gamma$ TRUPATH biosensor (Olsen et al., 2020), we directly proved that GPR17 is coupled to Gαi, and its activation could dissociate G$\beta\gamma$ from Gαi. Therefore, we conclude that GPR17 functions as a brake to negatively modulate nutrient-stimulated GLP-1 secretion by inhibiting cAMP and Ca^{2+} signaling through Gai and G$\beta\gamma$ subunits.

Limitations of the study

There are limitations with our current studies. First, the nature of the endogenous ligand(s) for GPR17 is still unclear. Several groups have performed initial studies on defining GPR17 ligands. Candidates include uracil nucleotides, cysteinyl leukotrienes (CysLTs), and other synthetic compounds (Ciana et al., 2006; Hennen et al., 2013; Parravicini et al., 2010; Parravicini et al., 2008; Pugliese et al., 2009). Although results were inconsistent among these studies (Simon et al., 2017), cysteinyl-leukotriene receptor (CysLTR) inhibitors did consistently show antagonistic activity for GPR17 signaling (Hennen et al., 2013; Merten et al., 2018), which raises the possibility of endogenous GPR17 agonists sharing structural similarity with cysteinyl leukotrienes, a class of inflammatory lipids. Although beyond the scope of our current study, identifying the endogenous Gpr17 ligand will provide valuable insights to Gpr17 biology and warrants future investigation. Second, not all GPR17-positive cells were stained positive for GLP-1, suggesting GPR17 may regulate other gut hormone secretion in different types of EECs. It remains to be determined whether or how Gpr17 signaling impacts the secretion of other gut hormones in EECs. We acknowledge that the increased GLP-1 secretion in knockout animals *in vivo* and intestinal organoid cultures *in vitro* may be one of the mechanisms leading to better glucose homeostasis. Other enteroendocrine mechanisms may also contribute to the glucose phenotype, which warrants future investigation. Third, we observed sexual dimorphism in glucose tolerance after long-term knockout. Sex differences in metabolic regulation have been well documented in animal and human studies (Gannon et al., 2018; Tramunt et al., 2020), such as the landmark paper revealing the essential role of incretin hormones in the double incretin receptor knockout (DIRKO) mice (Hansotia et al., 2004). Sexual dimorphism was observed in three aspects of glucose metabolism dependent or independent of the incretin receptors genetic knockout. First, female and male single and double incretin receptor knockout mice displayed different degrees of impaired glucose tolerance during the oral and intraperitoneal glucose tolerance tests. Second, islets isolated from female and male DIRKO mice showed different degrees of impaired glucose-stimulated first and second phase insulin secretion during the perifusion experiment. Third, islets isolated from female mice had half of the islet insulin content of the male counterparts, regardless of the genotypic differences. Likewise, human studies reported women exhibited more insulin secretion for a given glucose load (Basu et al., 2017; Basu et al., 2006; Horie et al., 2018). At the molecular level, sex hormones have been reported to regulate GLP-1 secretion. Estradiol positively regulates proglucagon-derived peptide secretion in mouse and human alpha and L cells (Handgraaf et al., 2018). Testosterone binding to androgen receptor enhances cAMP production and the incretin effect on insulin secretion in islet beta cells (Navarro et al., 2016). Though we cannot pinpoint the exact mechanism for the sex differences we observed after long-term Gpr17 genetic ablation in this study, we will address the potential interaction of Gpr17 and gonadal hormones in molecular signaling pathways and its implication for cellular physiological function in gut and islet tissues in future studies.

In conclusion, our results demonstrated the role of GPR17 signaling in the gut epithelium related to incretin secretion and the regulation of glucose metabolism. Additional insights into GPR17 biology may lead to more targeted therapies for T2D and obesity.

STAR★METHODS

Detailed methods are provided in the online version of this paper and include the following:

- KEY RESOURCES TABLE
- RESOURCE AVAILABILITY
  - Lead contact
  - Materials availability
  - Data and code availability
- EXPERIMENTAL MODEL AND SUBJECT DETAILS
  - Human intestinal samples
  - Animals
  - Cell lines
- METHOD DETAILS
  - qRT-PCR
  - Immunohistochemistry staining
  - Fluorescence-activated cell sorting (FACS) of *Gcg*-expressing cells in mouse gut epithelium
  - oGSIS *in vivo*
  - Glucose tolerance tests
  - Small intestine and colon histology
  - Gut incretins secretion *in vivo*
  - Mouse intestinal organoids culture
  - GLP-1 and GIP secretion studies in intestinal organoids
  - Whole-cell patch clamp
  - GloSensor cAMP assay
  - Bioluminescence resonance energy transfer (BRET) assay
  - Microbiome analysis
- QUANTIFICATION AND STATISTICAL ANALYSIS

AUTHOR CONTRIBUTIONS

S.Y. and H.R. designed and conducted experiments, analyzed data, and wrote and revised the manuscript. J.C. and A.R. designed and performed GloSensor cAMP assay and BRET assay, and helped with tissue collection and manuscript revision. S.A. performed GPR17 immunohistochemistry using

permeabilized and nonpermeabilized cells during revision. N.S. performed the metabolic phenotyping. A.E. performed the microbiota analysis with data interpretation. C.K. provided human gut samples from deceased donors. T.K., A.M., and C.E. provided equipment with technical training and revised the manuscript. H.R. conceived and supervised the study. All authors reviewed and approved the manuscript.

REFERENCES

Basu, A., Dube, S., and Basu, R. (2017). Men are from mars, women are from venus: Sex differences in insulin action and secretion. Adv. Exp. Med. Biol. *1043*, 53–64. https://doi.org/10.1007/978-3-319-70178-3_4.

Basu, R., Dalla Man, C., Campioni, M., Basu, A., Klee, G., Toffolo, G., Cobelli, C., and Rizza, R.A. (2006). Effects of age and sex on postprandial glucose metabolism: Differences in glucose turnover, insulin secretion, insulin action, and hepatic insulin extraction. Diabetes *55*, 2001–2014. https://doi.org/10.2337/db05-1692.

Bean, B.P. (1989). Neurotransmitter inhibition of neuronal calcium currents by changes in channel voltage dependence. Nature *340*, 153–156. https://doi.org/10.1038/340153a0.

Bolyen, E., Rideout, J.R., Dillon, M.R., Bokulich, N.A., Abnet, C.C., Al-Ghalith, G.A., Alexander, H., Alm, E.J., Arumugam, M., Asnicar, F., et al. (2019). Reproducible, interactive, scalable and extensible microbiome data science using QIIME 2. Nat. Biotechnol. *37*, 852–857. https://doi.org/10.1038/s41587-019-0209-9.

Bouchi, R., Foo, K.S., Hua, H., Tsuchiya, K., Ohmura, Y., Sandoval, P.R., Ratner, L.E., Egli, D., Leibel, R.L., and Accili, D. (2014). FOXO1 inhibition yields functional insulin-producing cells in human gut organoid cultures. Nat. Commun. *5*, 4242. https://doi.org/10.1038/ncomms5242.

Brubaker, P.L., Schloos, J., and Drucker, D.J. (1998). Regulation of glucagon-like peptide-1 synthesis and secretion in the GLUTag enteroendocrine cell line. Endocrinology *139*, 4108–4114. https://doi.org/10.1210/endo.139.10.6228.

Buccioni, M., Marucci, G., Dal Ben, D., Giacobbe, D., Lambertucci, C., Soverchia, L., Thomas, A., Volpini, R., and Cristalli, G. (2011). Innovative functional cAMP assay for studying G protein-coupled receptors: Application to the pharmacological characterization of GPR17. Purinergic Signal *7*, 463–468. https://doi.org/10.1007/s11302-011-9245-8.

Burmeister, M.A., Ayala, J.E., Smouse, H., Landivar-Rocha, A., Brown, J.D., Drucker, D.J., Stoffers, D.A., Sandoval, D.A., Seeley, R.J., and Ayala, J.E. (2017). The Hypothalamic glucagon-like peptide 1 receptor is sufficient but not necessary for the regulation of energy balance and glucose homeostasis in mice. Diabetes *66*, 372–384. https://doi.org/10.2337/db16-1102.

Callahan, B.J., McMurdie, P.J., Rosen, M.J., Han, A.W., Johnson, A.J., and Holmes, S.P. (2016). DADA2: High-resolution sample inference from illumina amplicon data. Nat. Methods *13*, 581–583. https://doi.org/10.1038/nmeth.3869.

Campbell, J.E., and Drucker, D.J. (2013). Pharmacology, physiology, and mechanisms of incretin hormone action. Cell Metab *17*, 819–837. https://doi.org/10.1016/j.cmet.2013.04.008.

Caporaso, J.G., Lauber, C.L., Walters, W.A., Berg-Lyons, D., Lozupone, C.A., Turnbaugh, P.J., Fierer, N., and Knight, R. (2011). Global patterns of 16S rRNA diversity at a depth of millions of sequences per sample. Proc. Natl. Acad. Sci. United States America *108*, 4516–4522. https://doi.org/10.1073/pnas.1000080107.

Ceruti, S., Villa, G., Genovese, T., Mazzon, E., Longhi, R., Rosa, P., Bramanti, P., Cuzzocrea, S., and Abbracchio, M.P. (2009). The P2Y-like receptor GPR17 as a sensor of damage and a new potential target in spinal cord injury. Brain : A J. Neurol. *132*, 2206–2218. https://doi.org/10.1093/brain/awp147.

Chambers, A.P., Sandoval, D.A., and Seeley, R.J. (2013). Integration of satiety signals by the central nervous system. Curr. Biol. *23*, R379–R388. https://doi.org/10.1016/j.cub.2013.03.020.

Chambers, A.P., Sorrell, J.E., Haller, A., Roelofs, K., Hutch, C.R., Kim, K.S., Gutierrez-Aguilar, R., Li, B., Drucker, D.J., D'Alessio, D.A., et al. (2017). The role of pancreatic preproglucagon in glucose homeostasis in mice. Cell Metab *25*, 927–934.e923. https://doi.org/10.1016/j.cmet.2017.02.008.

Chen, Y., Wu, H., Wang, S., Koito, H., Li, J., Ye, F., Hoang, J., Escobar, S.S., Gow, A., Arnett, H.A., et al. (2009). The oligodendrocyte-specific G protein-coupled receptor GPR17 is a cell-intrinsic timer of myelination. Nat. Neurosci. *12*, 1398–1406. https://doi.org/10.1038/nn.2410.

Ciana, P., Fumagalli, M., Trincavelli, M.L., Verderio, C., Rosa, P., Lecca, D., Ferrario, S., Parravicini, C., Capra, V., Gelosa, P., et al. (2006). The orphan receptor GPR17 identified as a new dual uracil nucleotides/cysteinyl-leukotrienes receptor. EMBO J. *25*, 4615–4627. https://doi.org/10.1038/sj.emboj.7601341.

Conley, Jason, Sun, Hongmao, Ayers, Kristin, Zhu, Hu, Chen, Rong, Shen, Min, Hall, Matthew, and Ren, Hongxia (2021). Human GPR17 missense variants identified in metabolic disease patients have distinct downstream signaling profiles. Journal of Biological Chemistry *297* (1), 100881. https://doi.org/10.1016/j.jbc.2021.100881.

Douros, J.D., Tong, J., and D'Alessio, D.A. (2019). The effects of bariatric surgery on islet function, insulin secretion, and glucose control. Endocr. Rev. *40*, 1394–1423. https://doi.org/10.1210/er.2018-00183.

Drucker, D.J., Jin, T., Asa, S.L., Young, T.A., and Brubaker, P.L. (1994). Activation of proglucagon gene transcription by protein kinase-A in a novel mouse enteroendocrine cell line. Mol. Endocrinol. *8*, 1646–1655. https://doi.org/10.1210/mend.8.12.7535893.

Drucker, D.J., and Nauck, M.A. (2006). The incretin system: Glucagon-like peptide-1 receptor agonists and dipeptidyl peptidase-4 inhibitors in type 2 diabetes. Lancet *368*, 1696–1705. https://doi.org/10.1016/s0140-6736(06)69705-5.

Dunlap, K., Luebke, J.I., and Turner, T.J. (1995). Exocytotic Ca2+ channels in mammalian central neurons. Trends Neurosci. *18*, 89–98.

el Marjou, F., Janssen, K.P., Chang, B.H., Li, M., Hindie, V., Chan, L., Louvard, D., Chambon, P., Metzger, D., and Robine, S. (2004). Tissue-specific and inducible cre-mediated recombination in the gut epithelium. Genesis *39*, 186–193. https://doi.org/10.1002/gene.20042.

Ericsson, A.C., Gagliardi, J., Bouhan, D., Spollen, W.G., Givan, S.A., and Franklin, C.L. (2018). The influence of caging, bedding, and diet on the composition of the microbiota in different regions of the mouse gut. Scientific Rep. *8*, 4065. https://doi.org/10.1038/s41598-018-21986-7.

Ezcurra, M., Reimann, F., Gribble, F.M., and Emery, E. (2013). Molecular mechanisms of incretin hormone secretion. Curr. Opin. Pharmacol. *13*, 922–927. https://doi.org/10.1016/j.coph.2013.08.013.

Gannon, M., Kulkarni, R.N., Tse, H.M., and Mauvais-Jarvis, F. (2018). Sex differences underlying pancreatic islet biology and its dysfunction. Mol. Metab. *15*, 82–91. https://doi.org/10.1016/j.molmet.2018.05.017.

Ghanem, S.S., Heinrich, G., Lester, S.G., Pfeiffer, V., Bhattacharya, S., Patel, P.R., DeAngelis, A.M., Dai, T., Ramakrishnan, S.K., Smiley, Z.N., et al. (2016). Increased glucose-induced secretion of glucagon-like peptide-1 in mice lacking the carcinoembryonic antigen-related cell adhesion molecule 2 (CEACAM2). J. Biol. Chem. *291*, 980–988. https://doi.org/10.1074/jbc.M115.692582.

Gribble, F.M., and Reimann, F. (2016). Enteroendocrine cells: Chemosensors in the intestinal epithelium. Annu. Rev. Physiol. *78*, 277–299. https://doi.org/10.1146/annurev-physiol-021115-105439.

Haber, A.L., Biton, M., Rogel, N., Herbst, R.H., Shekhar, K., Smillie, C., Burgin, G., Delorey, T.M., Howitt, M.R., Katz, Y., et al. (2017). A single-cell survey of the

small intestinal epithelium. Nature *551*, 333–339. https://doi.org/10.1038/nature24489.

Habib, A.M., Richards, P., Cairns, L.S., Rogers, G.J., Bannon, C.A., Parker, H.E., Morley, T.C., Yeo, G.S., Reimann, F., and Gribble, F.M. (2012). Overlap of endocrine hormone expression in the mouse intestine revealed by transcriptional profiling and flow cytometry. Endocrinology *153*, 3054–3065. https://doi.org/10.1210/en.2011-2170.

Handgraaf, S., Dusaulcy, R., Visentin, F., Philippe, J., and Gosmain, Y. (2018). 17-β Estradiol regulates proglucagon-derived peptide secretion in mouse and human α- and L cells. JCI Insight *3*. https://doi.org/10.1172/jci.insight.98569.

Hansotia, T., Baggio, L.L., Delmeire, D., Hinke, S.A., Yamada, Y., Tsukiyama, K., Seino, Y., Holst, J.J., Schuit, F., and Drucker, D.J. (2004). Double incretin receptor knockout (DIRKO) mice reveal an essential role for the enteroinsular axis in transducing the glucoregulatory actions of DPP-IV inhibitors. Diabetes *53*, 1326–1335. https://doi.org/10.2337/diabetes.53.5.1326.

Hauser, A.S., Attwood, M.M., Rask-Andersen, M., Schioth, H.B., and Gloriam, D.E. (2017). Trends in GPCR drug discovery: New agents, targets and indications. Nat. Rev. Drug Discov. *16*, 829–842. https://doi.org/10.1038/nrd.2017.178.

Hennen, S., Wang, H., Peters, L., Merten, N., Simon, K., Spinrath, A., Blattermann, S., Akkari, R., Schrage, R., Schroder, R., et al. (2013). Decoding signaling and function of the orphan G protein-coupled receptor GPR17 with a small-molecule agonist. Sci. Signal *6*, ra93. https://doi.org/10.1126/scisignal.2004350.

Holst, J.J. (2007). The physiology of glucagon-like peptide 1. Physiol. Rev. *87*, 1409–1439. https://doi.org/10.1152/physrev.00034.2006.

Horie, I., Abiru, N., Eto, M., Sako, A., Akeshima, J., Nakao, T., Nakashima, Y., Niri, T., Ito, A., Nozaki, A., et al. (2018). Sex differences in insulin and glucagon responses for glucose homeostasis in young healthy Japanese adults. J. Diabetes Investig. *9*, 1283–1287. https://doi.org/10.1111/jdi.12829.

Husted, A.S., Trauelsen, M., Rudenko, O., Hjorth, S.A., and Schwartz, T.W. (2017). GPCR-mediated signaling of metabolites. Cell Metab *25*, 777–796. https://doi.org/10.1016/j.cmet.2017.03.008.

Ikeda, S.R., and Dunlap, K. (1999). Voltage-dependent modulation of N-type calcium channels: Role of G protein subunits. Adv. Second Messenger Phosphoprotein Res. *33*, 131–151. https://doi.org/10.1016/s1040-7952(99)80008-1.

Inoue, A., Raimondi, F., Kadji, F.M.N., Singh, G., Kishi, T., Uwamizu, A., Ono, Y., Shinjo, Y., Ishida, S., Arang, N., et al. (2019). Illuminating G-protein-coupling selectivity of GPCRs. Cell *177*, 1933–1947.e1925. https://doi.org/10.1016/j.cell.2019.04.044.

Katsurada, K., and Yada, T. (2016). Neural effects of gut- and brain-derived glucagon-like peptide-1 and its receptor agonist. J. Diabetes Investig. *7*, 64–69. https://doi.org/10.1111/jdi.12464.

Kechin, A., Boyarskikh, U., Kel, A., and Filipenko, M. (2017). cutPrimers: A new tool for accurate cutting of primers from reads of targeted next generation sequencing. J. Comput. Biol. *24*, 1138–1143. https://doi.org/10.1089/cmb.2017.0096.

Kim, K.S., Seeley, R.J., and Sandoval, D.A. (2018). Signalling from the periphery to the brain that regulates energy homeostasis. Nat. Rev. Neurosci. *19*, 185–196. https://doi.org/10.1038/nrn.2018.8.

Kuhre, R.E., Frost, C.R., Svendsen, B., and Holst, J.J. (2015). Molecular mechanisms of glucose-stimulated GLP-1 secretion from perfused rat small intestine. Diabetes *64*, 370–382. https://doi.org/10.2337/db14-0807.

Lecca, D., Trincavelli, M.L., Gelosa, P., Sironi, L., Ciana, P., Fumagalli, M., Villa, G., Verderio, C., Grumelli, C., Guerrini, U., et al. (2008). The recently identified P2Y-like receptor GPR17 is a sensor of brain damage and a new target for brain repair. PLoS one *3*, e3579. https://doi.org/10.1371/journal.pone.0003579.

Loy, A., Maixner, F., Wagner, M., and Horn, M. (2007). probeBase–an online resource for rRNA-targeted oligonucleotide probes: New features 2007. Nucleic Acids Res. *35*, D800–D804. https://doi.org/10.1093/nar/gkl856.

Lüscher, C., and Slesinger, P.A. (2010). Emerging roles for G protein-gated inwardly rectifying potassium (GIRK) channels in health and disease. Nat. Rev. Neurosci. *11*, 301–315. https://doi.org/10.1038/nrn2834.

Mace, O.J., Tehan, B., and Marshall, F. (2015). Pharmacology and physiology of gastrointestinal enteroendocrine cells. Pharmacol. Res. Perspect. *3*, e00155. https://doi.org/10.1002/prp2.155.

Madison, B.B., Dunbar, L., Qiao, X.T., Braunstein, K., Braunstein, E., and Gumucio, D.L. (2002). Cis elements of the villin gene control expression in restricted domains of the vertical (crypt) and horizontal (duodenum, cecum) axes of the intestine. J. Biol. Chem. *277*, 33275–33283. https://doi.org/10.1074/jbc.M204935200.

Marschallinger, J., Schäffner, I., Klein, B., Gelfert, R., Rivera, F.J., Illes, S., Grassner, L., Janssen, M., Rotheneichner, P., Schmuckermair, C., et al. (2015). Structural and functional rejuvenation of the aged brain by an approved anti-asthmatic drug. Nat. Commun. *6*, 8466. https://doi.org/10.1038/ncomms9466.

Mastaitis, J., Min, S., Elvert, R., Kannt, A., Xin, Y., Ochoa, F., Gale, N.W., Valenzuela, D.M., Murphy, A.J., Yancopoulos, G.D., and Gromada, J. (2015). GPR17 gene disruption does not alter food intake or glucose homeostasis in mice. Proc. Natl. Acad. Sci. United States America *112*, 1845–1849. https://doi.org/10.1073/pnas.1424968112.

Mawla, A.M., and Huising, M.O. (2019). Navigating the depths and avoiding the shallows of pancreatic islet cell transcriptomes. Diabetes *68*, 1380–1393. https://doi.org/10.2337/dbi18-0019.

Merten, N., Fischer, J., Simon, K., Zhang, L., Schröder, R., Peters, L., Letombe, A.G., Hennen, S., Schrage, R., Bödefeld, T., et al. (2018). Repurposing HAMI3379 to block GPR17 and promote rodent and human oligodendrocyte differentiation. Cell Chem Biol *25*, 775–786.e775. https://doi.org/10.1016/j.chembiol.2018.03.012.

Michel, M.C., Wieland, T., and Tsujimoto, G. (2009). How reliable are G-protein-coupled receptor antibodies? Naunyn Schmiedebergs Arch. Pharmacol. *379*, 385–388. https://doi.org/10.1007/s00210-009-0395-y.

Mojsov, S., Heinrich, G., Wilson, I.B., Ravazzola, M., Orci, L., and Habener, J.F. (1986). Preproglucagon gene expression in pancreas and intestine diversifies at the level of post-translational processing. J. Biol. Chem. *261*, 11880–11889.

Moolenbeek, C., and Ruitenberg, E.J. (1981). The "Swiss roll": A simple technique for histological studies of the rodent intestine. Lab Anim. *15*, 57–59.

Nauck, M., Stockmann, F., Ebert, R., and Creutzfeldt, W. (1986). Reduced incretin effect in type 2 (non-insulin-dependent) diabetes. Diabetologia *29*, 46–52. https://doi.org/10.1007/BF02427280.

Navarro, G., Xu, W., Jacobson, D.A., Wicksteed, B., Allard, C., Zhang, G., De Gendt, K., Kim, S.H., Wu, H., Zhang, H., et al. (2016). Extranuclear actions of the androgen receptor enhance glucose-stimulated insulin secretion in the male. Cell Metab *23*, 837–851. https://doi.org/10.1016/j.cmet.2016.03.015.

Olsen, R.H.J., DiBerto, J.F., English, J.G., Glaudin, A.M., Krumm, B.E., Slocum, S.T., Che, T., Gavin, A.C., McCorvy, J.D., Roth, B.L., and Strachan, R.T. (2020). TRUPATH, an open-source biosensor platform for interrogating the GPCR transducerome. Nat. Chem. Biol. *16*, 841–849. https://doi.org/10.1038/s41589-020-0535-8.

Ou, Z., Ma, Y., Sun, Y., Zheng, G., Wang, S., Xing, R., Chen, X., Han, Y., Wang, J., Lu, Q.R., et al. (2019). A GPR17-cAMP-lactate signaling axis in oligodendrocytes regulates whole-body metabolism. Cell Rep. *26*, 2984–2997.e2984. https://doi.org/10.1016/j.celrep.2019.02.060.

Panaro, B.L., Tough, I.R., Engelstoft, M.S., Matthews, R.T., Digby, G.J., Moller, C.L., Svendsen, B., Gribble, F., Reimann, F., Holst, J.J., et al. (2014). The melanocortin-4 receptor is expressed in enteroendocrine L cells and regulates the release of peptide YY and glucagon-like peptide 1 in vivo. Cell Metab *20*, 1018–1029. https://doi.org/10.1016/j.cmet.2014.10.004.

Pang, Z.P., and Südhof, T.C. (2010). Cell biology of Ca2+-triggered exocytosis. Curr. Opin. Cell Biol *22*, 496–505. https://doi.org/10.1016/j.ceb.2010.05.001.

Parravicini, C., Abbracchio, M.P., Fantucci, P., and Ranghino, G. (2010). Forced unbinding of GPR17 ligands from wild type and R255I mutant receptor

models through a computational approach. BMC Struct. Biol. *10*. https://doi.org/10.1186/1472-6807-10-8.

Parravicini, C., Ranghino, G., Abbracchio, M.P., and Fantucci, P. (2008). GPR17: Molecular modeling and dynamics studies of the 3-D structure and purinergic ligand binding features in comparison with P2Y receptors. BMC Bioinformatics *9*, 263. https://doi.org/10.1186/1471-2105-9-263.

Pruesse, E., Quast, C., Knittel, K., Fuchs, B.M., Ludwig, W., Peplies, J., and Glockner, F.O. (2007). SILVA: A comprehensive online resource for quality checked and aligned ribosomal RNA sequence data compatible with ARB. Nucleic Acids Res. *35*, 7188–7196. https://doi.org/10.1093/nar/gkm864.

Pugliese, A.M., Trincavelli, M.L., Lecca, D., Coppi, E., Fumagalli, M., Ferrario, S., Failli, P., Daniele, S., Martini, C., Pedata, F., and Abbracchio, M.P. (2009). Functional characterization of two isoforms of the P2Y-like receptor GPR17: [35S]GTPgammaS binding and electrophysiological studies in 1321N1 cells. Am. J. Physiol. Cell Physiol *297*, C1028-C1040. https://doi.org/10.1152/ajpcell.00658.2008.

Qian, S., Chen, H., Weingarth, D., Trumbauer, M.E., Novi, D.E., Guan, X., Yu, H., Shen, Z., Feng, Y., Frazier, E., et al. (2002). Neither agouti-related protein nor neuropeptide Y is critically required for the regulation of energy homeostasis in mice. Mol. Cell Biol *22*, 5027–5035. https://doi.org/10.1128/mcb.22.14.5027-5035.2002.

Quigley, E.M. (2013). Gut bacteria in health and disease. Gastroenterol. Hepatol. (N Y) *9*, 560–569.

Reilly, A.M., Zhou, S., Panigrahi, S.K., Yan, S., Conley, J.M., Sheets, P.L., Wardlaw, S.L., and Ren, H. (2019). Gpr17 deficiency in POMC neurons ameliorates the metabolic derangements caused by long-term high-fat diet feeding. Nutr. Diabetes *9*, 29. https://doi.org/10.1038/s41387-019-0096-7.

Reimann, F., Maziarz, M., Flock, G., Habib, A.M., Drucker, D.J., and Gribble, F.M. (2005). Characterization and functional role of voltage gated cation conductances in the glucagon-like peptide-1 secreting GLUTag cell line. J. Physiol. *563*, 161–175. https://doi.org/10.1113/jphysiol.2004.076414.

Reimann, F., Tolhurst, G., and Gribble, F.M. (2012). G-protein-coupled receptors in intestinal chemosensation. Cell Metab *15*, 421–431. https://doi.org/10.1016/j.cmet.2011.12.019.

Ren, H., Cook, J.R., Kon, N., and Accili, D. (2015). Gpr17 in AgRP Neurons regulates feeding and sensitivity to insulin and leptin. Diabetes *64*, 3670–3679. https://doi.org/10.2337/db15-0390.

Ren, H., Orozco, I.J., Su, Y., Suyama, S., Gutierrez-Juarez, R., Horvath, T.L., Wardlaw, S.L., Plum, L., Arancio, O., and Accili, D. (2012). FoxO1 target Gpr17 activates AgRP neurons to regulate food intake. Cell *149*, 1314–1326, S0092-8674(12)00577-6 [pii]. https://doi.org/10.1016/j.cell.2012.04.032.

Robichaux, W.G., 3rd, and Cheng, X. (2018). Intracellular cAMP sensor EPAC: Physiology, pathophysiology, and therapeutics development. Physiol. Rev. *98*, 919–1053. https://doi.org/10.1152/physrev.00025.2017.

Rogers, G.J., Tolhurst, G., Ramzan, A., Habib, A.M., Parker, H.E., Gribble, F.M., and Reimann, F. (2011). Electrical activity-triggered glucagon-like peptide-1 secretion from primary murine L-cells. J. Physiol. *589*, 1081–1093. https://doi.org/10.1113/jphysiol.2010.198069.

Ruiz-Velasco, V., and Ikeda, S.R. (2000). Multiple G-protein betagamma combinations produce voltage-dependent inhibition of N-type calcium channels in rat superior cervical ganglion neurons. J. Neurosci. : Official J. Soc. Neurosci. *20*, 2183–2191. https://doi.org/10.1523/jneurosci.20-06-02183.2000.

Satin, L.S. (2000). Localized calcium influx in pancreatic beta-cells: its significance for Ca2+-dependent insulin secretion from the islets of Langerhans. Endocrine *13*, 251–262. https://doi.org/10.1385/ENDO:13:3:251.

Sato, T., Vries, R.G., Snippert, H.J., van de Wetering, M., Barker, N., Stange, D.E., van Es, J.H., Abo, A., Kujala, P., Peters, P.J., and Clevers, H. (2009). Single Lgr5 stem cells build crypt-villus structures in vitro without a mesenchymal niche. Nature *459*, 262–265. https://doi.org/10.1038/nature07935.

Schwartz, G.J., and Zeltser, L.M. (2013). Functional organization of neuronal and humoral signals regulating feeding behavior. Annu. Rev. Nutr. *33*, 1–21. https://doi.org/10.1146/annurev-nutr-071812-161125.

Scrocchi, L.A., Brown, T.J., MaClusky, N., Brubaker, P.L., Auerbach, A.B., Joyner, A.L., and Drucker, D.J. (1996). Glucose intolerance but normal satiety in mice with a null mutation in the glucagon-like peptide 1 receptor gene. Nat. Med. *2*, 1254–1258. https://doi.org/10.1038/nm1196-1254.

Scrocchi, L.A., and Drucker, D.J. (1998). Effects of aging and a high fat diet on body weight and glucose tolerance in glucagon-like peptide-1 receptor -/- mice. Endocrinology *139*, 3127–3132. https://doi.org/10.1210/endo.139.7.6092.

Seino, S., and Shibasaki, T. (2005). PKA-dependent and PKA-independent pathways for cAMP-regulated exocytosis. Physiol. Rev. *85*, 1303–1342. https://doi.org/10.1152/physrev.00001.2005.

Shiota, C., Prasadan, K., Guo, P., Fusco, J., Xiao, X., and Gittes, G.K. (2017). Gcg (CreERT2) knockin mice as a tool for genetic manipulation in pancreatic alpha cells. Diabetologia *60*, 2399–2408. https://doi.org/10.1007/s00125-017-4425-x.

Simon, K., Hennen, S., Merten, N., Blattermann, S., Gillard, M., Kostenis, E., and Gomeza, J. (2016). The orphan G protein-coupled receptor GPR17 negatively regulates oligodendrocyte differentiation via Galphai/o and its downstream effector molecules. J. Biol. Chem. *291*, 705–718. https://doi.org/10.1074/jbc.M115.683953.

Simon, K., Merten, N., Schroder, R., Hennen, S., Preis, P., Schmitt, N.K., Peters, L., Schrage, R., Vermeiren, C., Gillard, M., et al. (2017). The orphan receptor GPR17 is unresponsive to uracil nucleotides and cysteinyl leukotrienes. Mol. Pharmacol. *91*, 518–532. https://doi.org/10.1124/mol.116.107904.

Smrcka, A.V. (2008). G protein βγ subunits: Central mediators of G protein-coupled receptor signaling. Cell Mol. Life Sci. : CMLS *65*, 2191–2214. https://doi.org/10.1007/s00018-008-8006-5.

Steinert, R.E., Feinle-Bisset, C., Asarian, L., Horowitz, M., Beglinger, C., and Geary, N. (2017). Ghrelin, CCK, GLP-1, and PYY(3-36): Secretory controls and physiological roles in eating and glycemia in health, obesity, and after RYGB. Physiol. Rev. *97*, 411–463. https://doi.org/10.1152/physrev.00031.2014.

Sun, Q.Q., Huguenard, J.R., and Prince, D.A. (2001). Neuropeptide Y receptors differentially modulate G-protein-activated inwardly rectifying K+ channels and high-voltage-activated Ca2+ channels in rat thalamic neurons. J. Physiol. *531*, 67–79. https://doi.org/10.1111/j.1469-7793.2001.0067j.x.

Tong, X., Kono, T., Anderson-Baucum, E.K., Yamamoto, W., Gilon, P., Lebeche, D., Day, R.N., Shull, G.E., and Evans-Molina, C. (2016). SERCA2 deficiency impairs pancreatic β-cell function in response to diet-induced obesity. Diabetes *65*, 3039–3052. https://doi.org/10.2337/db16-0084.

Tramunt, B., Smati, S., Grandgeorge, N., Lenfant, F., Arnal, J.F., Montagner, A., and Gourdy, P. (2020). Sex differences in metabolic regulation and diabetes susceptibility. Diabetologia *63*, 453–461. https://doi.org/10.1007/s00125-019-05040-3.

Walters, W.A., Caporaso, J.G., Lauber, C.L., Berg-Lyons, D., Fierer, N., and Knight, R. (2011). PrimerProspector: de novo design and taxonomic analysis of barcoded polymerase chain reaction primers. Bioinformatics *27*, 1159–1161. https://doi.org/10.1093/bioinformatics/btr087.

Wang, Y.J., and Kaestner, K.H. (2019). Single-Cell RNA-Seq of the pancreatic islets–a promise not yet fulfilled? Cell Metab *29*, 539–544. https://doi.org/10.1016/j.cmet.2018.11.016.

Yan, S., Kubal, C., and Ren, H. (2021). Dataset for Confocal Study of G Protein-Coupled Receptors 17 (GPR17), Chromogranin A (CHGA), Glucagon-like Peptide-1 (GLP-1) and Glucose-dependent Insulinotropic Polypeptide (GIP) in Human Intestine (IUPUI University Library). https://doi.org/10.7912/D2/22.

Zietek, T., Rath, E., Haller, D., and Daniel, H. (2015). Intestinal organoids for assessing nutrient transport, sensing and incretin secretion. Scientific Rep. *5*, 16831. https://doi.org/10.1038/srep16831.

STAR★METHODS

KEY RESOURCES TABLE

REAGENT or RESOURCE	SOURCE	IDENTIFIER
Antibodies		
Rabbit polyclonal anti-GPR17 (1:200)	Novus	Cat#NLS4229; RRID: AB_2232678
Mouse monoclonal anti-Chromogranin A (1:200)	Santa Cruz Biotechnology	SC-393941; RRID: AB_2801371
Mouse monoclonal anti-GIP (1:100)	Abcam	Cat# ab30679, RRID: AB_2109682
Mouse monoclonal anti-GLP1 (1:50)	Novus	Cat# NBP1-50697, RRID: AB_11016296
Mouse monoclonal anti-HA (1:1000)	BioLegend	Cat# 901513, RRID: AB_2565335
Goat anti-Rabbit IgG (H+L) (1:500)	Thermo Fisher Scientific	Cat# A-21428, RRID: AB_2535849
Goat anti-Mouse IgG (H+L) (1:500)	Thermo Fisher Scientific	Cat# 35502, RRID: AB_844397
Biological samples		
Human gut tissue	IU Health Methodist Hospital	NA
Chemicals, peptides, and recombinant proteins		
Aprotinin	Sigma-Aldrich	A6279; CAS: 9087-70-1
DPP-IV inhibitor	Millipore	Cat#DPP4-010
Exendin-3 (9-39) amide (Ex9)	Tocris	2081; CAS: 133514-43-9
Forskolin	Tocris	1099; CAS: 66575-29-9
IBMX	Sigma-Aldrich	I7018; CAS: 28822-58-4
MDL29,951	Laboratory of Donald Landry and Andrew Wasmuth	NA
Pertussis toxin (PTX)	Sigma-Aldrich	P2980; CAS: 70323-44-3
Tamoxifen	Sigma-Aldrich	T5648; CAS: 10540-29-1
Tetrodotoxin (TTX)	Tocris	1069; CAS: 18660-81-6
Y27632	STEMCELL Technologies	Cat#72302
NT(8-13)	Sigma-Aldrich	N5266; CAS: 60482-95-3
Critical commercial assays		
GLP-1 ELISA kit	Meso Scale Discovery	Cat#K1503PD-1
GIP ELISA kit	Millipore	Cat#EZRMGIP-55K
Insulin ELISA kit	Millipore	Cat#EZRMI-13K
TRUPATH kit	Gift from Bryan Roth	Addgene#1000000163
Deposited data		
Mouse Fecal Microbiome Data	This paper	SRA: PRJNA756295
IHC raw images and quantified data	This paper	https://doi.org/10.7912/D2/22
Experimental models: Cell lines		
HEK293	ATCC	CRL-1573
GLUTag	Gift from Sonia M. Najjar	NA
HELA	ATCC	CCL-2
Experimental models: Organisms/strains		
Mouse: B6.Cg-$Gt(ROSA)^{26Sortm9(CAG-tdTomato)Hze}$/J	The Jackson Laboratory	CAT#007909
Mouse: B6.Cg-Tg(Vil1-cre)997Gum/J	The Jackson Laboratory	CAT#004586
Mouse: B6;129S-$Gcg^{tm1.1(cre/ERT2)Gkg}$/J	The Jackson Laboratory	CAT#030681
Mouse: B6.Cg-Tg(Vil1-cre/ERT2)23Syr/J	The Jackson Laboratory	CAT#020282

(Continued on next page)

Continued

REAGENT or RESOURCE	SOURCE	IDENTIFIER
Mouse: *Gpr17^fl/fl*	Columbia University Transgenic Mouse Core Facility	NA
Oligonucleotides		
See Table S1 for a list of all primers and oligonucleotides	This paper	NA
Recombinant DNA		
pcDNA3.1 (−)	(Conley et al., 2021)	NA
pcDNA3.1-mGpr17-GFP	(Conley et al., 2021)	NA
pcDNA3.1-HA-hGPR17	(Conley et al., 2021)	NA
pcDNA3.1(+)-hNT1R	CDNA	NTSR100000
pcDNA3-HA-mGPR17	This paper	NA
pGloSensor^TM-22F	Promega	E2301
Software and algorithms		
pClamp 10.7	Molecular Devices	NA
Prism 9	GraphPad	NA

RESOURCE AVAILABILITY

Lead contact
Further information and requests for resources and reagents should be directed to and will be fulfilled by the Lead Contact, Hongxia Ren (renh@iu.edu).

Materials availability
All unique/stable reagents generated in this study are available from the Lead Contact with a completed Materials Transfer Agreement.

Data and code availability
Mouse fecal microbiome data have been deposited at NCBI Bioproject and are publicly available as of the date of publication. Accession number is listed in the key resources table. IHC raw images and quantified data have been deposited at IU DataWorks and are publicly available as of the date of publication. DOI is listed in the key resources table. This paper does not report original code. Any additional information required to reanalyze the data reported in this paper is available from the lead contact upon request.

EXPERIMENTAL MODEL AND SUBJECT DETAILS

Human intestinal samples
Human gut full thickness biopsies were obtained from two deceased donors (male, aged 26 and 30 years old) by transplant surgeon at IU School of Medicine during organ procurements. Fresh samples were maintained and transported in cold DMEM/F12 medium (Invitrogen, Carlsbad, CA); and processed for qRT-PCR within 24 h after resection. Human jejunum and colon were fixed in 4% PFA for 24 h and sectioned for immunohistochemistry staining. Consent for research was obtained from the next of kin of deceased donors by Indiana Donor Network. The study was reviewed and Indiana University Human Research Protection Program (IU HRPP) staff determined the project is not human subjects research and does not require further IU Institutional Review Boards (IRB) review.

Animals
B6.Cg-*Gt(ROSA)26Sor^tm9(CAG-tdTomato)Hze*/J (#007909, *Rosa-tdTomato*), B6.Cg-Tg(*Vil1-cre*)997Gum/J (#004586, *Vil1-Cre*), and B6; 129S-*Gcg^tm1.1(cre/ERT2)Gkg*/J (#030681, *Gcg-CreERT*) mice were purchased from the Jackson Laboratory (JAX). *Vil1Cre-ER^T2* mice were kindly shared by Dr. Lori Sussel. *Gpr17^fl/fl* mice were generated as described before (Ren et al., 2015) and were bred with *Vil1-Cre* mice (Madison et al., 2002) to generate control WT (*Gpr17^fl/fl*) and constitutive intestine-specific Gpr17 knockouts (*Gpr17^fl/fl;Vil1Cre*). Inducible intestine-specific Gpr17 knockouts (iKO) were generated by mating *Vil1Cre-ER^T2* mice (el el Marjou et al., 2004) with *Gpr17^fl/fl* mice. *Gcg* expressing-dependent tdTomato reporter mice were generated by mating *Rosa-tdTomato* with *Gcg-CreERT* mice. Cre recombinase was activated by oral gavage of 10 mg/mL tamoxifen (Sigma-Aldrich, St. Louis, MO)/corn oil solution (200 μL/mouse/day) for 5 consecutive days. Experiments were conducted using

3~16-month-old male and female mice as indicated in the figure legends. All animals were bred and housed under specific pathogen-free conditions and handled in accordance with the guidelines for animal care of Indiana University School of Medicine Animal Care and Use Committee.

Cell lines
Murine enteroendocrine cells, GLUTag cells, were kindly made available to the community by Dr. Daniel J. Drucker (Toronto, Canada) and cultured in Dulbecco's modified Eagle's medium (DMEM) containing 1 g/L glucose, as described previously (Ghanem et al., 2016). HEK293 cells and HeLa cells were cultured in Minimum Essential Medium (MEM), 10% fetal bovine serum (FBS), and 1x Penicillin-Streptomycin solution and maintained at 37°C and 5% CO2.

METHOD DETAILS

qRT-PCR
Gut segment dissection was performed as previously described (Panaro et al., 2014). In brief, gut was removed from the stomach to the rectum. Segments measuring 1 cm were removed from the glandular stomach (distal end), duodenum (adjacent to the pyloric sphincter), jejunum (halfway between the pyloric sphincter and the ileocecal valve), ileum (3 cm above the ileocecal valve), and colon (halfway between the cecocolic junction and anus). Total RNA for gut segments were extracted by Trizol (Invitrogen) and reverse transcribed with Superscript II reverse transcriptase (Invitrogen). We performed quantitative real-time PCR (qRT-PCR) in CFX Connect Real-Time system (Bio-Rad, Hercules, CA) using primers spanning introns. Primer sequences are listed in Table S1.

Immunohistochemistry staining
Immunohistochemistry staining of human small intestine (jejunum) and colon were performed by using antibodies for GPR17 (NLS4229; Novus, Centennial, CO), Chromogranin A (SC-393941; Santa Cruz Biotechnology, Dallas, Texas), GIP (ab30679; abcam, Cambridge, MA) and GLP-1 (NBP1-50697; Novus). Images and quantified results were deposited in IU DataWorks (Yan et al., 2021). Insulin and glucagon staining in pancreatic sections were performed by CDMD islets core facility using methods described previously (Tong et al., 2016).

GPR17 antibody was validated in HEK293 cells and HeLa cells transiently transfected by pcDNA3.1-HA-hGPR17 plasmids. Cells were transfected with pcDNA3.1-HA-hGPR17 plasmids for overnight. GPR17 (NLS4229; Novus) and HA (#901513; Biolegend, San Diego, CA) antibodies were used for immunostaining. Cells were permeabilized by 0.1% Triton X-100 for total GPR17 staining or non-permeabilized for cell-surface GPR17 staining. Chamber slides were imaged under LSM-700 confocal microscope (ZEISS, Oberkochen, Germany). 10-22 randomly selected cells per image and total 10 images were quantified for staining intensity by using Image J (NIH).

Fluorescence-activated cell sorting (FACS) of *Gcg*-expressing cells in mouse gut epithelium
The whole colon and the last quarter of the small intestine from *Gcg-CreERT;Rosa-tdTomato* mice were isolated and rinsed in cold PBS. Intestine epithelium tissues were collected by scraping and resuspended in TrypLE Express (Thermo Fisher Scientific, Waltham, MA) at 37°C for 20 min to dissociate into single cell suspension. Cells were re-suspended in 1mL 1X PBS containing 1% BSA and 10 μM Y27632 (STEMCELL Technologies, Cambridge, MA). Cells were stained by DAPI before subjected to flow cytometry sorting by FACSAria 2 SORP (Becton Dickinson, Franklin Lakes, NJ) and data were analyzed on FACSDiva 8.0.1 software (Becton Dickinson). Forward scatter and size scatter were used to get single cells based on granularity and height. DAPI negative gate was used to get live cells. tdTomato positive cells with a fluorescence signal measured above 10^3 were gated to collect the Gcg-CreERT positive (i.e. GLP-1-producing) cells. We collected the tdTomato-positive (T+), and tdTomato-negative (T-) live cells for RNA extraction with Trizol LS reagent (Invitrogen).

oGSIS *in vivo*
Adult mice were fasted overnight. Insulin levels (#EZRMI-13K; Millipore, Burlington, MA) were measured in tail serum samples collected before and 15 min after oral glucose (3 g/kg) administration.

Glucose tolerance tests
Adult mice were fasted for overnight or 4-6 h for glucose tolerance tests. Tail blood glucose levels were measured by AlphaTRAK2 glucose meter at 0, 15, 30, 60, 90, 120 min after glucose administration via intraperitoneal (i.p.) injection or oral gavage. The dose of glucose for each experiment was noted in the figure legends.

Small intestine and colon histology
The mouse entire small intestine (SI), from the gastric pylorus to the ileocecal valve, and the colon, from cecocolic junction to anus, were dissected from anaesthetized mice (3-4 months old). The SI and colon were opened longitudinally and wrapped as a "Swiss roll" (Moolenbeek and Ruitenberg, 1981), respectively. Swiss rolls were fixed in 4% paraformaldehyde (PFA) for 24-48 h, cryoprotected with 30% sucrose (w/v PBS), and sectioned (10 μm) for H&E staining.

Gut incretins secretion *in vivo*

Adult mice were given glucose (3 g/kg) via oral gavage after being deprived of food for 4-6 h. Tail blood was collected from tail at 0min and 10 min after glucose administration. Blood was collected and mixed with an inhibitor cocktail (Aprotinin, A6279, Sigma-Aldrich; DPP-IV inhibitor, DPP4-010, Millipore; 0.5M EDTA, AM9261, Invitrogen. 1:1:1, 10 μL mixture for each sample.). On another occasion, tail blood was collected at 0 min and 60 min after 100% corn oil (10 μL/g BW) via oral gavage after 4∼6 h fasting. Total GIP (#EZRMGIP-55K; Millipore) and total GLP-1 (#K1503PD-1; MSD, Rockville, MD) measurements were measured in plasma samples.

Mouse intestinal organoids culture

Mouse intestinal organoids were cultured in mouse IntesiCultTM Organoid Growth Medium (STEMCELL Technologies, Cambridge, MA) by following the manufacturer's instruction. 20 cm of small intestine proximal to stomach were harvested for culturing intestinal organoids, as this region allows optimal efficiency for generating organoids (Zietek et al., 2015). Organoids were used for experiments after two passages from primary culture or frozen.

GLP-1 and GIP secretion studies in intestinal organoids

Intestinal organoids were cultured in 24-well plates with a density of 200-300 organoids per well for 7-10 days. Secretion experiments were performed by incubating the organoids with test regents in treated solution (138 mM NaCl, 4.5 mM KCl, 4.2 mM NaHCO$_3$, 1.2 mM NaH$_2$PO$_4$, 2.5 mM CaCl$_2$, 1.2 mM MgCl$_2$, and 10 mM HEPES supplemented with 0.1% (wt/vol) fatty acid-free BSA and 1% DPP-IV inhibitor, pH 7) for 2 h at 37°C. At the end of the incubation period, supernatant was collected, and the organoids were lysed in RIPA buffer supplemented with protease inhibitor and DPP-IV inhibitor. Incretins in supernatant and lysates were assayed using ELISA kit for GIP (#EZRMGIP-55K; Millipore) and total GLP-1 (#K1503PD-1; MSD). Secretion was first calculated as the percentage of secreted GLP-1 (supernatant) in total GLP1 (both supernatant and cell lysates) and then normalized to the basal secretion in WT organoids in parallel on the same day.

Whole-cell patch clamp

The voltage-gated Ca^{2+} currents in GLUTag cells were recorded by the standard whole-cell patch clamp with a procedure adapted from previous reports (Reimann et al., 2005; Rogers et al., 2011). Cells and plasmid (pcDNA3.1-mGpr17-GFP) mixture were cultured onto glass cover slips in 12-well plate. After overnight transfection, the medium was replaced with fresh growth medium, and the cells were subjected to patch clamp 1 day after that. Single cells and well-defined cells in small clusters were patched. GFP positive or negative cells were identified by using an upright microscope (E600FN, Nikon, Japan) fitted with fluorescence optics. Microelectrodes were pulled from borosilicate glass capillary (1B150F, WPI, Sarasota, FL) by a Micropipette Puller (P-1000, Sutter Instrument, Novato, CA) and had 4∼6 MΩ when filled with pipette solution. Recordings were acquired with an MultiClamp 700B (Molecular Devices, San Jose, CA), a DigiData 1322A (Molecular Devices) and analyzed with pClamp10 software (Molecular Devices). The bath solution contained (mmol/L): 4.5 CsCl, 118 NaCl, 4.2 NaHCO3, 1.2 NaH2PO4, 2.6 CaCl2, 1.2 MgCl2, 10 HEPES, 20 TEA, 1 glucose (pH7.4). The pipette solution contained (mmol/L): 107 CsCl, 1 CaCl2, 7MgCl2, 11 EGTA, 10 HEPES, 5 Na2ATP (pH7.4). Tetrodotoxin (TTX, 0.3 μmol/L) was added into the bath solution to block Na$^+$ currents.

GloSensor cAMP assay

GLUTag cells were transiently transfected with pGloSensor-cAMP-22F (Promega, Madison, WI) together with either pcDNA3.1(−) empty vector or pcDNA3-HA-mGpr17 (mGpr17) plasmids and cultured in poly-D-lysine coated 96-well plates. Transfection mix was replaced with fresh growth media the next day. The following day, growth media was removed, cells were washed with CO2-independent media (Gibco, Life Technologies Corporation, Grand Island, NY), and cells were loaded with equilibration buffer (CO2-independent media containing 2% GloSensor cAMP reagent) (Promega, Madison, WI) for 2 h at 37°C and 5% CO2. Cells were then allowed to equilibrate to ambient room temperature for 30 min. Luminescence was read at ambient room temperature every 2 minutes using a SpectraMax iD5 plate reader (Molecular Devices, San Jose, CA). Initial baseline luminescence was measured for 8 minutes. Subsequently, drug treatments were added to wells, followed by luminescence measurements. Specifically, luminescence was measured for 10 min following each of IBMX and MDL29,951 additions. Finally, forskolin was added and luminescence was measured for 30 min.

Data were expressed as the difference in RLU form the average initial baseline, divided by the average initial baseline for each individual well (ΔRLU/RLU) and represent the Mean ± SEM of two independent experiments performed with duplicate wells. Concentration response curves for MDL29,951 were from the 4 minute time point after MDL29,951 addition. Concentration response curves for MDL29,951 in the presence of 3 μM forskolin represent the average of the 16-30 min time points following forskolin addition.

Bioluminescence resonance energy transfer (BRET) assay

BRET assay was performed using TRUPATH biosensor (Addgene, Watertown, MA) as described previously (Olsen et al., 2020). HEK293 cells were seeded into 6-well plates at a density of 600,000 cells/well. The following day, cells were transiently transfected with 1:1:1:1 ratio of either pcDNA3.1(−) empty vector, pcDNA3.1(+)-hNT1R, or pcDNA3-HA-mGpr17 together with pcDNA5/FRT/TO-Gαi1-Rluc8, pcDNA3.1-Gβ3, and pcDNA3.1-Gγ9-GFP2 using Lipofectamine 3000. 24 h post-transfection, cells were dissociated

from the plate with 0.05% trypsin-EDTA, resuspended in MEM containing 1% FBS and seeded into poly-D-lysine-coated white, opaque, 96-well plates at 30,000 cells/well. The next day, cells were washed with Hank's balanced salt solution (HBSS)-based assay buffer (HBSS, 20 mM HEPES, pH 7.2), followed by addition of 80 μL/well assay buffer, and then loaded with 10 μL/well 50 μM coelenterazine 400a diluted in assay buffer for 5 min at ambient room temperature. 10 μL/well of the indicated treatments were added in triplicate and incubated for 5 min at room temperature before filtered luminescence was read at 410 nm and 515 nm on a SpectraMax iD5 plate reader. BRET ratios for each well were calculated as the ratio of luminescence emission at 515 nm divided by 410 nm. The net BRET response represents the BRET ratio for each well subtracted by the mean BRET ratio response of the vehicle-treated wells for each receptor transfection condition. Data were represented as the Mean $\pm$ SEM of three or four independent experiments performed with triplicate wells.

Microbiome analysis

Fresh fecal samples were collected in the morning during *ad libitum* feeding. Frozen fecal samples were sent to the University of Missouri for DNA isolation and 16S rRNA gene V4 sequencing using the Illumina MiSeq platform as previously described (Ericsson et al., 2018). Briefly, DNA was extracted using PowerFecal kits (Qiagen) according to the manufacturer's instructions, with the exception that samples were homogenized in the provided bead tubes using a TissueLyser II (Qiagen, Venlo, Netherlands) for 3 min at 30/s, rather than performing the initial homogenization of samples using the vortex adapter described in the protocol, before proceeding according to the protocol and eluting in 100 μL of elution buffer (Qiagen). DNA yields were quantified via fluorometry (Qubit 2.0, Invitrogen, Carlsbad, CA) using quant-iT BR dsDNA reagent kits (Invitrogen) and normalized to a uniform concentration and volume.

Extracted fecal DNA was processed at the University of Missouri DNA Core Facility. Bacterial 16S rRNA amplicons were constructed via amplification of the V4 region of the 16S rRNA gene with universal primers (U515F/806R) previously developed against the V4 region, flanked by Illumina standard adapter sequences (Caporaso et al., 2011; Walters et al., 2011). Oligonucleotide sequences are available at proBase (Loy et al., 2007). Dual-indexed F and R primers were used in all reactions. PCR was performed in 50 μL reactions containing 100 ng metagenomic DNA, primers (0.2 μM each), dNTPs (200 μM each), and Phusion high-fidelity DNA polymerase (1U, Thermo Fisher). Amplification parameters were $98^{\circ}C^{(3min)}$ + [$98^{\circ}C^{(15sec)}$ + $50^{\circ}C^{(30sec)}$ + $72^{\circ}C^{(30sec)}$] x 25 cycles +$72^{\circ}C^{(7min)}$. Amplicon pools (5 μL/reaction) were combined, mixed, and then purified by addition of Axygen^{TM} Axyprep MagPCR clean-up beads to an equal volume of 50 μL of amplicons and incubated for 15 min at room temperature (RT). Products were then washed multiple times with 80% ethanol and the dried pellet was resuspended in 32.5 μL EB buffer (Qiagen), incubated for 2 min at RT, and then placed on a magnetic stand for 5 min. The final amplicon pools were evaluated using an Advanced Analytical Fragment Analyzer automated electrophoresis system, quantified using quant-iT HS dsDNA kits, and diluted according to Illumina's standard protocol for sequencing as 2×250 bp paired-end reads on the MiSeq instrument.

DNA sequences were assembled and annotated at the MU Informatics Research Core Facility. Primers were designed to match the 5′ ends of the forward and reverse reads. Cutadapt (Kechin et al., 2017) (version 2.6; https://github.com/marcelm/cutadapt) was used to remove the primer from the 5′ end of the forward read. If found, the reverse complement of the primer to the reverse read was then removed from the forward read as were all bases downstream. Thus, a forward read could be trimmed at both ends if the insert was shorter than the amplicon length. The same approach was used on the reverse read, but with the primers in the opposite roles. Read pairs were rejected if one read or the other did not match a 5′ primer, and an error-rate of 0.1 was allowed. Two passes were made over each read to ensure removal of the second primer. A minimal overlap of three bp with the 3′ end of the primer sequence was required for removal. The QIIME2 (Bolyen et al., 2019) DADA2 (Callahan et al., 2016) plugin (version 1.10.0) was used to denoise, de-replicate, and count ASVs (amplicon sequence variants), incorporating the following parameters: 1) forward and reverse reads were truncated to 150 bases, 2) forward and reverse reads with number of expected errors higher than 2.0 were discarded, and 3) Chimeras were detected using the "consensus" method and removed. R version 3.5.1 and Biom version 2.1.7 were used in QIIME2. Taxonomies were assigned to final sequences using the Silva.v132 (Pruesse et al., 2007) database, using the classify-sklearn procedure.

QUANTIFICATION AND STATISTICAL ANALYSIS

We analyzed data with Student's t–test or one–way or two-way ANOVA using GraphPad Prism software. All of the statistical details of experiments can be found in the figure legends. No method was used to determine whether the data met assumptions of the statistical approach. We used the customary threshold of $p < 0.05$ to declare statistical significance.